Ionospheric Effects over the People's Republic of China from the Super-Powerful Tropospheric Western Pacific Phenomenon of September–October 2018: Results from Oblique Sounding

Leonid F. Chernogor[1, 2, 3], Kostiantyn P. Garmash[2], Qiang Guo[3]*, Victor T. Rozumenko[2], Yu Zheng[1]*

[1]Qingdao University, 308 Ningxia Road, Qingdao, 266071 China
e-mail: *zhengyu@qdu.edu.cn*
[2]V. N. Karazin Kharkiv National University, 4 Svobody Sq., Kharkiv, 61022 Ukraine
e-mail: *Leonid.F.Chernogor@gmail.com*
e-mail: *Garmash@karazin.ua*
e-mail: *vtrozumenko45@gmail.com*
[3]Harbin Engineering University, 145 Nantong Street, Nangang District, Harbin, 150001 China
e-mail: *guoqiang@hrbeu.edu.cn*

Correspondence to: Yu Zheng (zhengyu@qdu.edu.cn), Qingdao University, 308 Ningxia Road, Qingdao, 266071 China and Qiang Guo (guoqiang@hrbeu.edu.cn), Harbin Engineering University, 145 Nantong Street, Nangang District, Harbin, 150001 China.

Abstract. The paper deals with the effects that accompanied the Super Typhoon Kong-Rey action in the ionosphere over the People's Republic of China (PRC). The observations were made using the Harbin Engineering University, PRC, multifrequency multiple path coherent software defined radio system. The typhoon began on September 29, 2018, and ceased to exist on October 6, 2018. The ionospheric response to the super typhoon action was clearly observed to occur both on October 1–2, 2018 (when the typhoon was 2,800–3,300 km from the propagation path midpoints and its energy gained a maximum value) and on October 5–6, 2018 when the typhoon was 1,000–1,500 km from the midpoints and its energy decreased by a factor of about 4. The ionospheric effects are more pronounced along the nearest propagation paths, whereas no effect was detected along the propagation path at the farthest distance from the typhoon. The super typhoon action on the ionosphere was accompanied by the generation or amplification of quasi-sinusoidal variations in the Doppler shift by a factor of 2–3, as well as by noticeable variations in the signal amplitude. The Doppler spectra were observed to broaden in a number of cases. The period of wave perturbations exhibited variability in the ~20 min to ~120 min range, which suggests that the perturbations in the ionospheric electron density were caused by atmospheric gravity waves (AGWs) generated by the typhoon; in addition, the greater the AGW period, the greater the Doppler shift. As the period increased from 20 min to 120 min, the Doppler shift amplitudes increased from ~0.1 Hz to 0.5–1 Hz, whereas the amplitude of quasi-sinusoidal variations in the electron density increased from a 0.4 to 0.6 of per cent within the same range of the AGW periods. The Doppler measurements have shown that the dusk terminator and super typhoon acted synergistically to amplify the ionospheric response to these sources of energy.

1 Introduction

A violent tropical cyclone arising in the northwestern Pacific Ocean is termed the typhoon. In record-breaking typhoons, the atmospheric pressure drops down to 870 hPa, whereas the pressure deficit reaches 140 hPa, and the wind speed attains a maximum of 85 m/s, with 94 m/s maximum gusts.

Recent studies have shown that typhoons significantly influence the upper atmosphere, including the ionosphere. The coupling of the lower and upper atmosphere occurs via acoustic and atmospheric gravity waves (AGWs) generated by typhoons (Hung and Kuo, 1978; Kuester et al., 2008). Such a mechanism for coupling is naturally called the acoustic–gravity mechanism (Chernogor, 2006, 2012).

Typhoons are accompanied by water vapor condensation, the development of powerful convective lift, and the appearance of severe thunderstorms (Mikhailova et al., 2000, 2002). Lightning discharges act to generate electromagnetic emissions that may be capable of heating electrons and perturbing the electron density in the ionospheric D region (Nickolaenko and Hayakawa, 1995; Chernogor, 2006, 2012). The large enough fluxes of electromagnetic emissions lead to pitch angle scattering of energetic electrons in the radiation belts via wave-particle interaction, and consequently, part of the electrons precipitates into the lower ionosphere (Inan et al., 2007; Voss et al., 1984, 1998; Bortnik et al., 2006). As a result, secondary perturbations in the plasma conductivity (~100–150 km altitude) and in the geomagnetic and electric fields capable of affecting processes in the magnetosphere can arise. Such a mechanism should be considered the electromagnetic mechanism (Chernogor, 2006, 2012).

The increase in the quasi-stationary electric field may be of different origin (Mikhailova et al., 2000; Isaev et al., 2002, 2010; Sorokin et al., 2005; Pulinets et al., 2014). Localized ~10^{-9}–10^{-8} A/m^2 electric currents arise within thunderstorm clouds at 10–15 km altitude, which disturb the global electric circuit and increase by 1–2 orders of magnitude quasi-sinusoidal electric fields that are mapped to the ionosphere and magnetosphere and affect the motion of high-energy electrons trapped in the radiation belts. Under specified conditions, the precipitation of these electrons may occur into the ionosphere, and a repeated coupling between the subsystems in the ocean–atmosphere–ionosphere–magnetosphere (OAIM) system occur (Chernogor, 2006, 2012). This mechanism for coupling may by termed the electric mechanism (Chernogor, 2006, 2012).

Thus, powerful typhoons are capable of governing the coupling between the subsystems in the OAIM system. A lot of studies deal with the acoustic–gravity mechanism, and therefore this mechanism has been studied better than the others.

Prasad et al. (1975) were the first to ascertain the influence of meteorological processes, namely, a tropical cyclone on the ionosphere. Hung and Kuo (1978, 1985) described observations of the manifestations of the AGWs generated by hurricanes. Krishmam Raju et al. (1981) have studied the influence of infrasound generated by thunderstorms. Boška and Šauli (2001), Šindelarova et al. (2009), Chernigovskaya et al. (2015) described the observations of AGWs of meteorological origin.

Hickey et al. (2001, 2011), Kuester et al. (2008), Gavrilov and Kshevetskii (2015), Karpov and Kshevetskii (2017) studied the coupling of AGWs and the upper atmosphere theoretically.

Okuzawa et al. (1986), Xiao et al. (2007), Vanina–Dart et al. (2007), Afraimovich et al. (2008), Polyakova and Perevalova (2011, 2013), Zakharov and Kunitsyn (2012), Suzuki et al. (2013), Chou et al. (2017), Li et al. (2017, 2018), Chum et al. (2018), Zakharov et al. (2019, 2022) have studied the influence of typhoons and hurricanes on the upper atmosphere and discuss the major role AGWs play in coupling different atmospheric regions. These researchers invoked various measurement techniques for probing the ionosphere: GPS technology, ionosondes, rocket techniques, and HF Doppler technique.

Chernogor et al. (2021, 2022) have studied the ionospheric response to the super typhoons Hagibis, Ling-Ling, and Faxai. The main features of the variations in radio wave characteristics in the 5–10 MHz band have been determined, and aperiodic and quasi-sinusoidal perturbations in the electron density have been ascertained.

The effect of AGWs, sudden stratospheric warming events, variations in space weather, and of solar activity on the coupling between the subsystems in the atmosphere–ionosphere system has been analyzed in the review by Yiğit et al. (2016).

The results of recent observations are presented in papers by Kong et al. (2017), Li et al. (2018), Zhao et al. (2018), Song et al. (2019), Wen and Jin (2020), Chen et al. (2020), Ke et al. (2020), Zhao et al. (2020), Das et al. (2021), Freeshah et al. (2021), Chernogor et al. (2021, 2022), Zakharov et al. (2019, 2022).

The influence of typhoons on the ionosphere might be expected to significantly depend on typhoon parameters, local time, season, solar cycle changes, and on the state of atmospheric and space weather. To date, there remains insufficient knowledge about this influence and therefore the study of the ionospheric response to any new typhoon is of interest. In this paper, the Super Typhoon Kong-Rey, the most powerful worldwide typhoon in 2018, has been chosen to analyze the ionospheric response to the typhoon action.

The scientific objectives of this study is to reveal the processes that the typhoon–dusk terminator coupling brings into play, to derive specifications of wave periods and amplitudes of perturbations in the in the electron density, and to estimate the space scales of the perturbations launched by the super typhoon Kong-Rey event of September–October 2018 into the ionosphere over the People's Republic of China (PRC).The observations were made using the Harbin Engineering University, PRC, multifrequency multiple path coherent software defined radio system for probing the ionosphere at oblique incidence.

2 General information on the super typhoon Kong-Rey

Table 1 presents basic information on the Category 5 Super Typhon Kong-Rey; part of the information was retrieved from http://agora.ex.nii.ac.jp/digital-typhoon/summary/wnp/s/201825.html.en. It shows that the typhoon originated on September 29, 2018 and ceased to exist on October 6, 2018. The pressure reached a minimum value of 900 hPa, whereas the pressure deficit reached a maximum of 105 hPa (see also Figure 1). The wind speed attained a maximum of 215 km/h or 60 m/s, with 77 m/s maximum gusts. The largest radius of the storm wind attained 260 km, and the largest radius of the gale wind was observed to be 750 km. The length of the typhoon path is estimated to be 4,107 km, with an average speed of 23.6 km/h or 6.6 m/s. The dynamic wind pressure is estimated to attain 2.25 kPa, with 3.8 kPa maximum gust pressure. The kinetic energy of the rotating air was estimated to be close to 1.65×10^{18} J, whereas the mean power was estimated to attain 1.7×10^{13} W. On

October 1 and 2, 2018, the super typhoon energy was a maximum, and the typhoon approached 600 km off the shores of the
100   PRC on October 2, 2018 (Figure 1). On October 5, 2018, the typhoon was 250 km off the shores of the PRC, when the
pressure deficit was observed to be ~30 hPa.

Table 1. Basic Parameters of the Super Typhoon Kong-Rey (Courtesy of Asanobu KITAMOTO, Digital Typhoon,
National Institute of Informatics, Japan).

Birth	2018-09-29 06:00:00 UTC
Death	2018-10-06 12:00:00 UTC
Lifetime	174 h/7.250 days
Minimum Pressure	900 hPa
Pressure Maximum Deficit	105 hPa
Maximum Wind Speed	215 km/h (60 m/s)
Largest Radius of Storm Wind	260 km
Largest Radius of Gale Wind	750 km
Length of Movement	4,107 km
Average Speed	23.6 km/h (6.56 m/s)
Range of Movement	Latitude 25.3°: Longitude 16.7°
Typhoon Kinetic Energy	1.65×10^{18} J
Typhoon Power	1.7×10^{13} W
Rainfall	250–300 mm/h
Maximum Pressure Drop	–25 hPa / 6 h; –40 hPa / 12 h –65 hPa / 24 h; –96 hPa / 48 h
Data Start	2018-09-28 00:00:00 UTC
Data End	2018-10-07 12:00:00 UTC
Data Duration	228 h / 9.500 days

3 Analysis of the state of space weather

105   Before the ionospheric response to the super typhoon action can be detected, it is necessary to perform a comprehensive
analysis of space weather.

Figure 2 accumulates knowledge regarding the state of space weather during the super typhoon Kong-Rey event.
First, consider the parameters of the solar wind (retrieved from https://omniweb.gsfc.nasa.gov/form/dx1.html). Under quiet
conditions, the proton number density is observed to be close to 5×10^6 m^{-3}, whereas on September 29, 2018, and October 1,
110   3, and 5, 2018, it shows increases up to $(15–20) \times 10^6$ m^{-3}. On September 26 and 30, 2018, as well on October 3–4, 2018, the
plasma flow speed increases from ~400 km/s to 500–520 km/s. During the same UT period, plasma temperature increases
from $\sim(2–3) \times 10^4$ K to $\sim(1.2–1.5) \times 10^5$ K, whereas the dynamic solar wind pressure increases from ~1 nPa to 4–5 nPa. The

B_y component of the interplanetary magnetic field exhibits temporal variability within the –5.9 nT to 11.6 nT limits, while the B_z component changes from –4.7 nT to 4.0 nT.
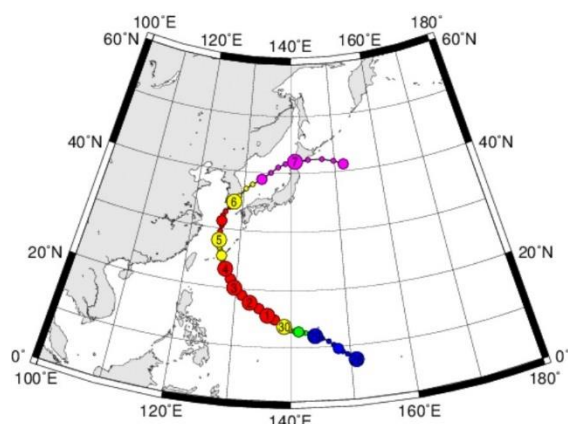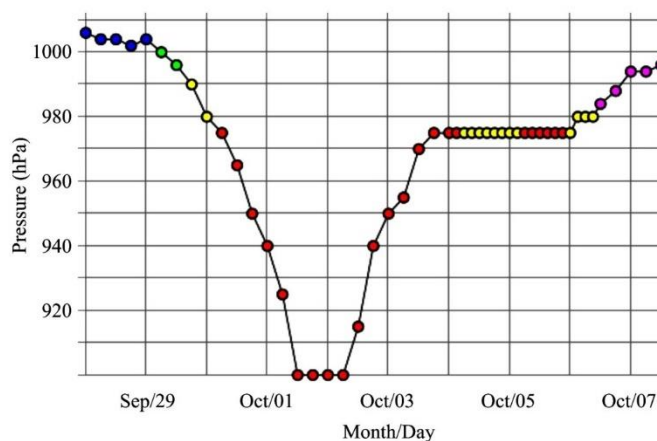
Figure 1: Super Typhoon Kong-Rey (a) trajectory and (b) pressure. (Courtesy of Asanobu KITAMOTO, Digital Typhoon, National Institute of Informatics, Japan).

On September 26 and 29, 2018, as well as on October 1, 3–4, 2018, the calculated energy input, ε_A, into the Earth's magnetosphere from the solar wind showed increases up to ~5 GJ/s.

The K_p index sporadically exhibited increases to 3.0–3.7, whereas the D_{st} index showed fluctuations from –16 nT to 16 nT.

Table 2 presents temporal variations in the $F_{10.7}$ index for the September 26 to October 09, 2018, period.

During the typhoon Kong-Rey event, solar activity and the state of space weather were conducive to observing the ionospheric effects from the typhoon. Only on October 7, 2018, a moderate magnetic storm started, with $K_{pmax} = 5.3$, and $D_{stmin} \approx -53$ nT.

4 Analysis of the State of the Ionosphere

The state of the ionosphere was monitored by the ionosonde nearest to Harbin, i.e., the WK546 URSI code ionosonde located in the city of Wakkanai (45.16°N, 141.75°E) in Japan (Guo et al., 2019a, 2019b, 2020; Chernogor et al., 2020; Luo et al., 2020). Figure 3 shows UT variations in the main ionogram parameters. The minimum frequency, f_{min}, observed on ionograms exhibited fluctuations around 1.5 MHz. The critical frequencies of the E layer, f_{oE}, were close to 3 MHz during the day, and gradually decreased to 1.8–2.0 MHz in the evening hours. At night, measurements of f_{oE} were impossible. The blanketing frequency of the sporadic E layer, most often, showed fluctuations within the 3–8 MHz limits, however sometimes it could attain 13–15 MHz. The ordinary-wave critical frequency f_oF_2 was observed to be 4–6 MHz during the day and to decrease to 3.0–3.5 MHz at night.
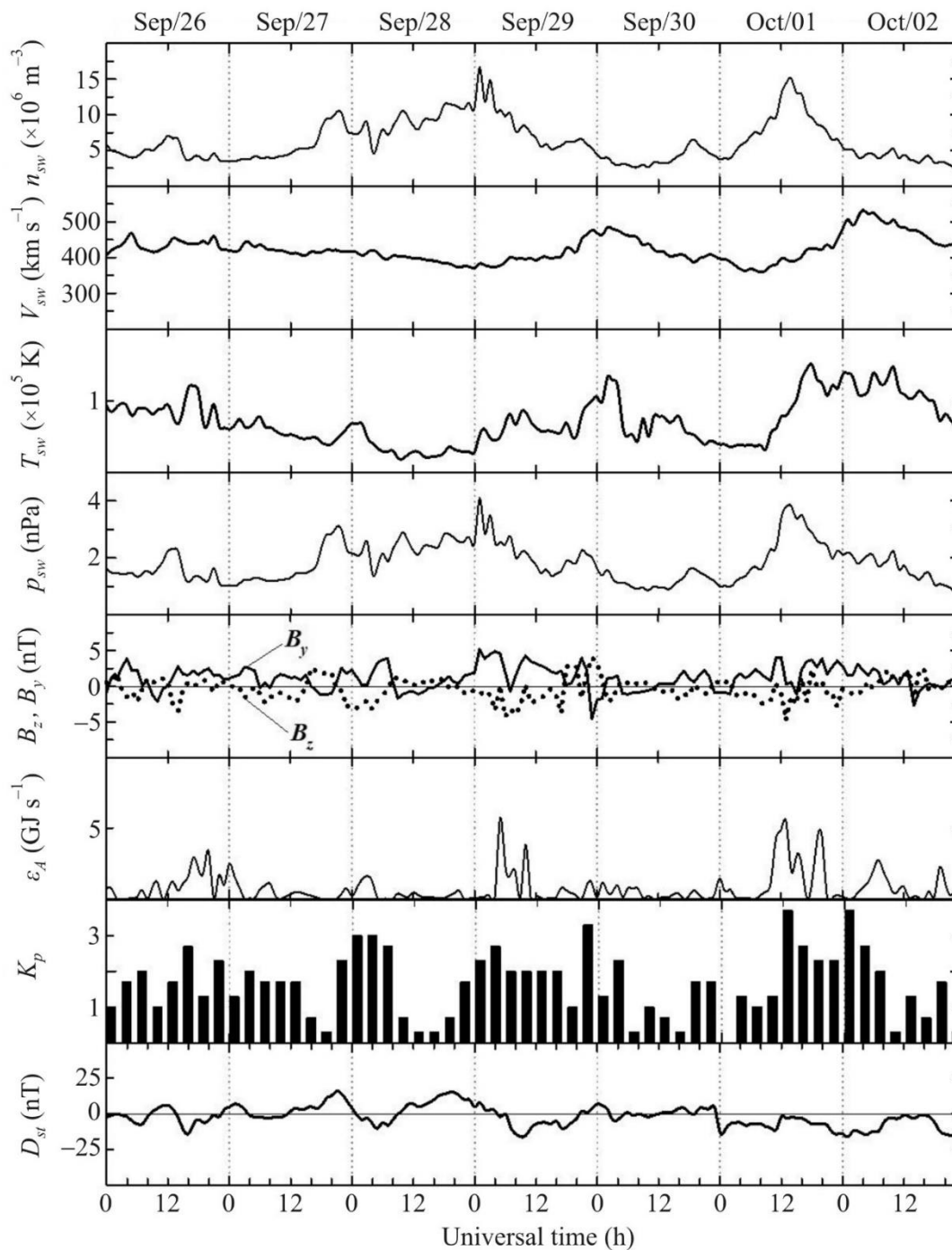
135

Figure 2: Universal time dependences of the solar wind parameters: proton number density n_{sw}, plasma flow speed V_{sw}, plasma temperature T_{sw}, dynamic solar wind pressure p_{sw}, B_z and B_y components of the interplanetary magnetic field, calculated energy input, ε_A, into the Earth's magnetosphere from the solar wind; and K_p- and D_{st}-indices for the September 26 – October 02, 2018 period.
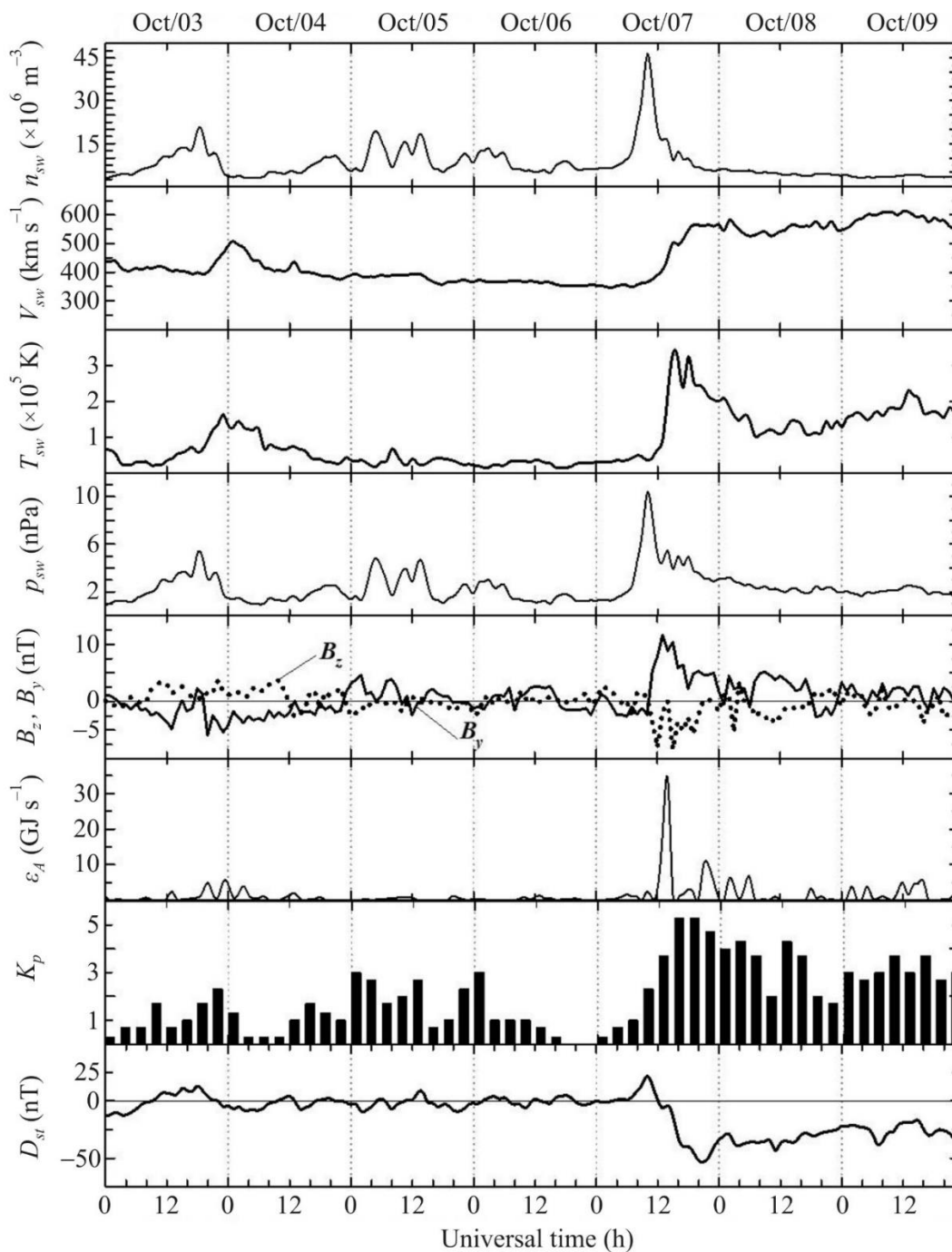
140

Figure 2: Continued for the October 03–09, 2018 period.

145

Table 2. Daily $F_{10.7}$ index for the September 26, 2018–October 09, 2018, period ()

Date (2018)	09/26	09/27	09/28	09/29	09/30	10/01	10/02	10/03	10/04	10/05	10/06	10/07	10/08	10/09
$F_{10.7}$	69.3	67.4	69.4	68.9	68.5	70.3	67.1	68.4	67.2	68.7	68.6	69.4	68.7	69.3
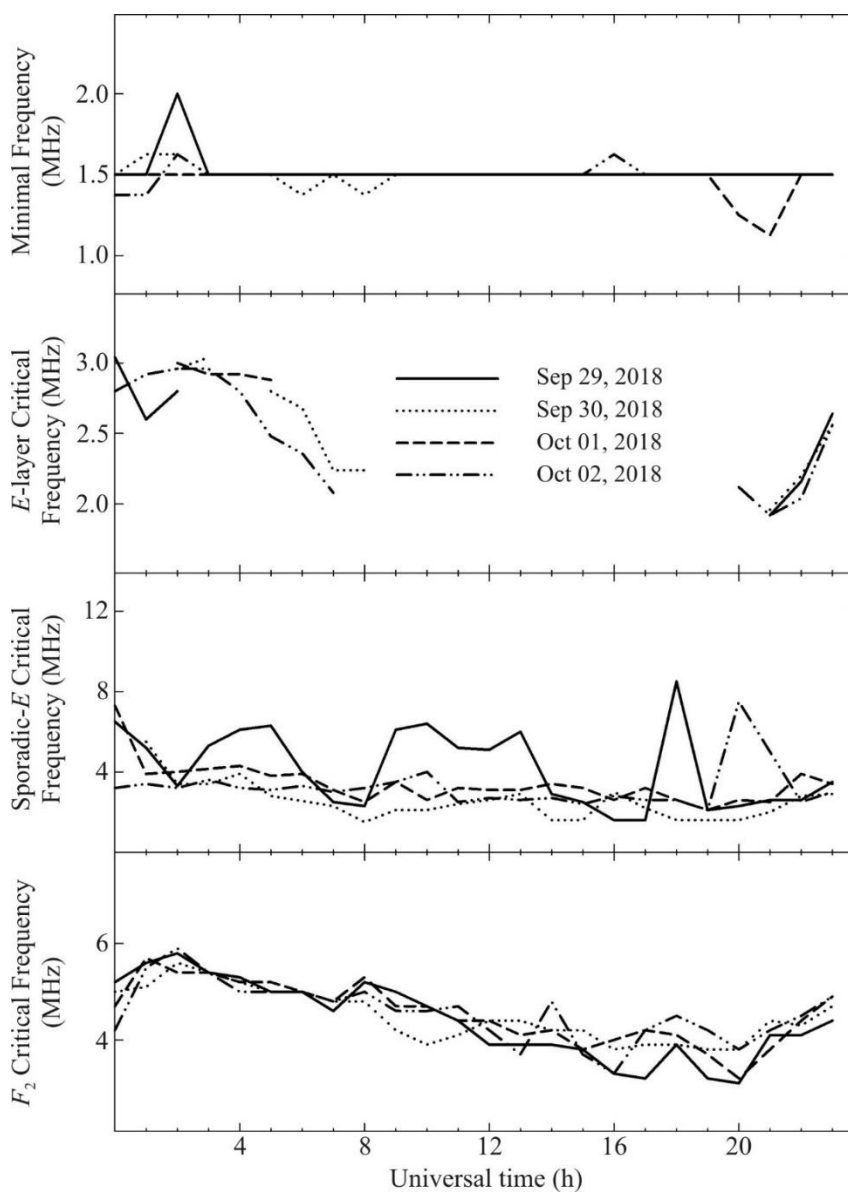
150 **Figure 3: Universal time variations in ionogram parameters: critical frequencies f_{min}, f_oE, f_oE_s, and f_oF_2 for the September 29–October 2, 2018, period.**
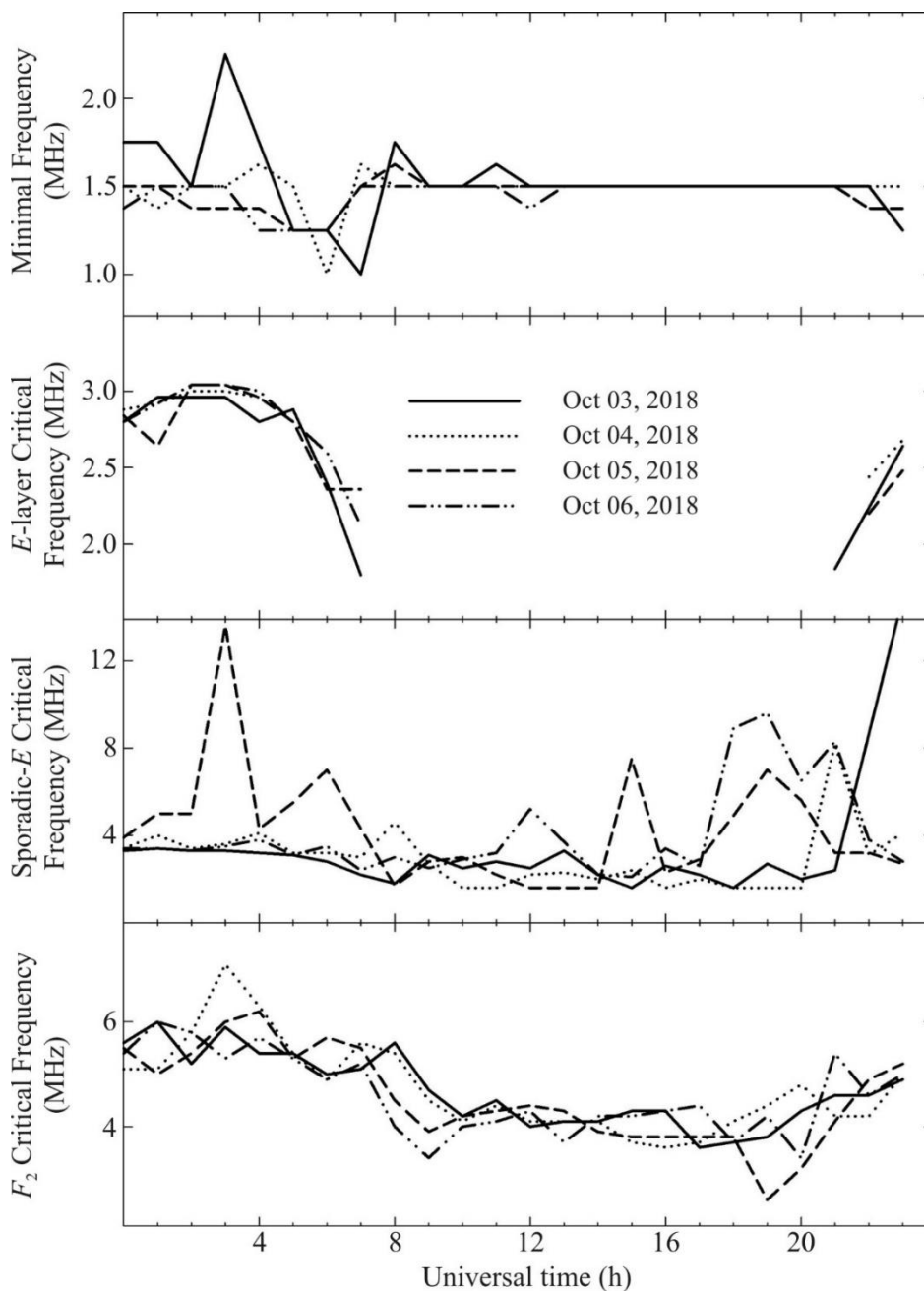
Figure 3: Continued for the October 3–6, 2018 period.

155

Figure 4 shows temporal variations in the virtual heights. The virtual heights h'_E are observed to vary mainly within the 95–105 km, whereas the virtual heights h'_{Es} most frequently show variations within the 90–110 km limits, which could sometimes exhibit an increase to 140–160 km.

5 Instrumentation and techniques

160 The study of the effects from the Super Typhoon was conducted using the Harbin Engineering University multifrequency multiple path coherent software defined radio system for probing the ionosphere at oblique incidence (Guo et al., 2019a, 2019b, 2020; Chernogor et al., 2020; Luo et al., 2020). The system utilizes radio transmissions of broadcasting stations located in the PRC, the Republic of Korea, Japan, the Russian Federation, and Mongolia, the signals of which are received and processed at the Harbin Engineering University campus (45.78°N, 126.68°E).

165 Continuous monitoring of the dynamic processes operating in the ionosphere is done along 14 propagation paths in the 5 – 10 MHz band (Table 3, Figure 5) as described by Guo et al. (2019a, 2019b, 2020), Chernogor et al. (2020), and Luo et al. (2020). In the event under study, post-analysis of the data acquired along six propagation paths has shown they are not suitable for processing.

 Monitoring the dynamic processes in the ionosphere is done via calculating the temporal dependences of the Doppler spectra and signal amplitudes. The Doppler spectra are used to plot the Doppler shift as a function of time, $f_D(t)$, for the main ray or for a few rays.

 Spectrum analysis is performed applying the autoregressive technique of Marple (1987), which provides a frequency resolution of 0.01 Hz over ~20 s intervals with 7.5 s time resolution.

 The $f_D(t)$ dependences are then used to calculate the trend $\overline{f}_D(t)$, the fluctuations $\delta f_D(t) = f_D(t) - \overline{f}_D(t)$, and the
175 systems spectral analysis is performed (Chernogor, 2008) over 60 – 280 min intervals to select harmonics in the $T \leq 5$ min and $T = 10 – 140$ min period ranges.

6 Ionospheric results from oblique incidence sounding

The post analysis of the data collected during the Super Typhoon Kong-Rey event has shown that the transmissions from only eight of the fourteen transmitters in the ~6–10 MHz band are suitable for studying the Super Typhoon Kong-Rey event
180 (Figure 5). The specifications of the transmitters and radio-wave propagation paths are presented in Table 3. Since the lengths of the propagation paths are found to be ~1000–2000 km and the frequencies of the sounding radio waves are relatively small, the sounding waves were reflected either from the E layer or from the sporadic E during the daytime when the Doppler shift, f_D, was observed to be ~0 Hz. Consequently, these measurements were ineffective at observing the ionospheric dynamics. At night, the radio waves were reflected from the ionospheric F region and only sometimes from the
185 sporadic E. The Doppler shift of the radio waves reflected from the F region exhibited variations from ~0.1 Hz to ~0.5 Hz and greater. Therefore, the measurements made during nights, evenings, and mornings could be used for studying ionospheric dynamics.

 The observations suffer another drawback: the transmitters of the broadcasting radio stations did not transmit continuously.
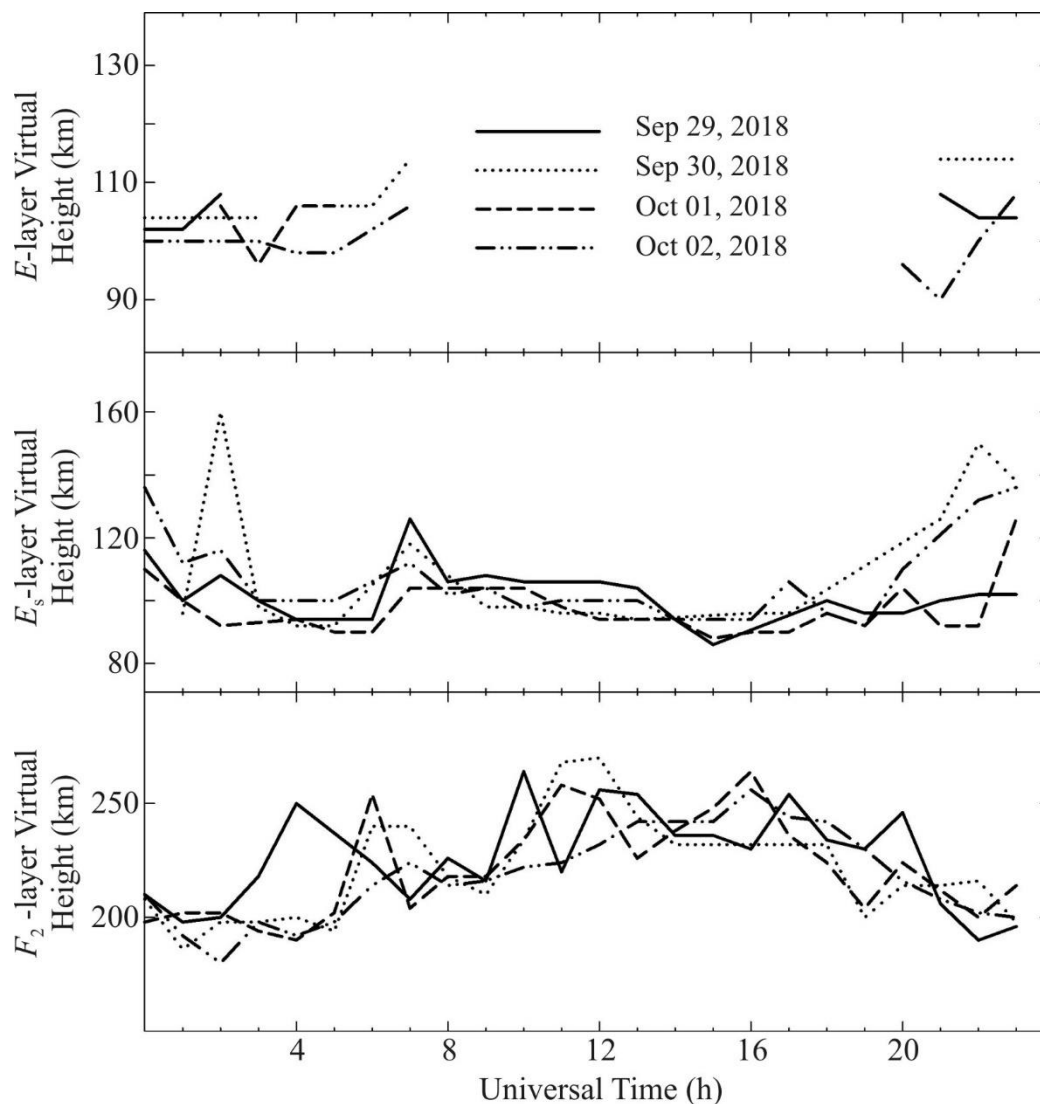
190

Figure 4: Universal time variations in ionogram parameters: virtual heights h'_E, h'_{Es}, and h'_{F2} for September 29–October 2, 2018, period.

6.1 Hwaseong to Harbin radio-wave propagation path

This transmitter operating at 6,015 kHz is located in the Republic of Korea at a great-circle range, R, of ~950 km from the

195   receiver; it was switched off from 00:00 UT to 03:30 UT.

On the reference days of September 29 and 30, 2018, the Doppler shift was observed to be less than $\pm(0.2–0.3)$ Hz (Figure 6). From 09:00 UT to 15:00 UT, the Doppler spectra showed diffuseness, and the Doppler shift exhibited quasi-sinusoidal variations with a ~20–30 min period, T, and a ~0.1–0.2 Hz amplitude, f_{Da}, respectively.
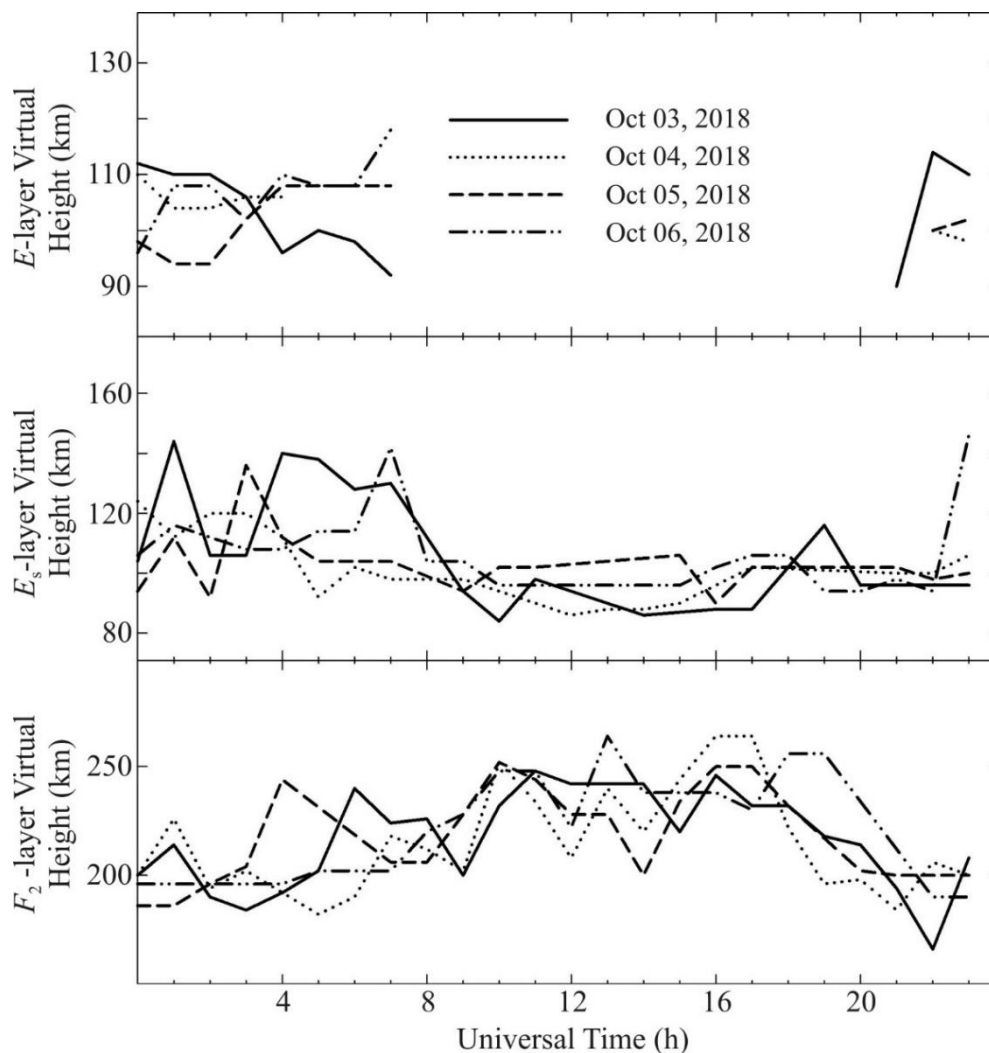
200

Figure 4: Continued for the October 2–6, 2018 period.

Doppler spectra broadening was absent during the interval from October 1 to 6, 2018. On October 1, 2018, $f_{Da} \approx 0.3$–0.5 Hz, and $T \approx 20$–120 min.

205 On October 2, 2018, the 20–80-min period amplitude of the Doppler shift did not exceed 0.1–0.3 Hz. A single 140-min period wavelet in f_{Da} up to 0.5 Hz took place on October 3, 2018. On October 4, 2018, the amplitude of the Doppler shift did not exceed 0.2 Hz, while observable quasi-sinusoidal processes were practically absent. On October 5 and 6, 2018, the Doppler shift exhibited sporadic increases up to 0.5–0.6 Hz and decreases down to –(0.5–0.7) Hz. For the rest of time, $f_{Da} \approx 0.1$ Hz, whereas $T \approx 20$–30 min.

210 The amplitudes of individual variations in the signal strength did not exceed 10–15 dBV.
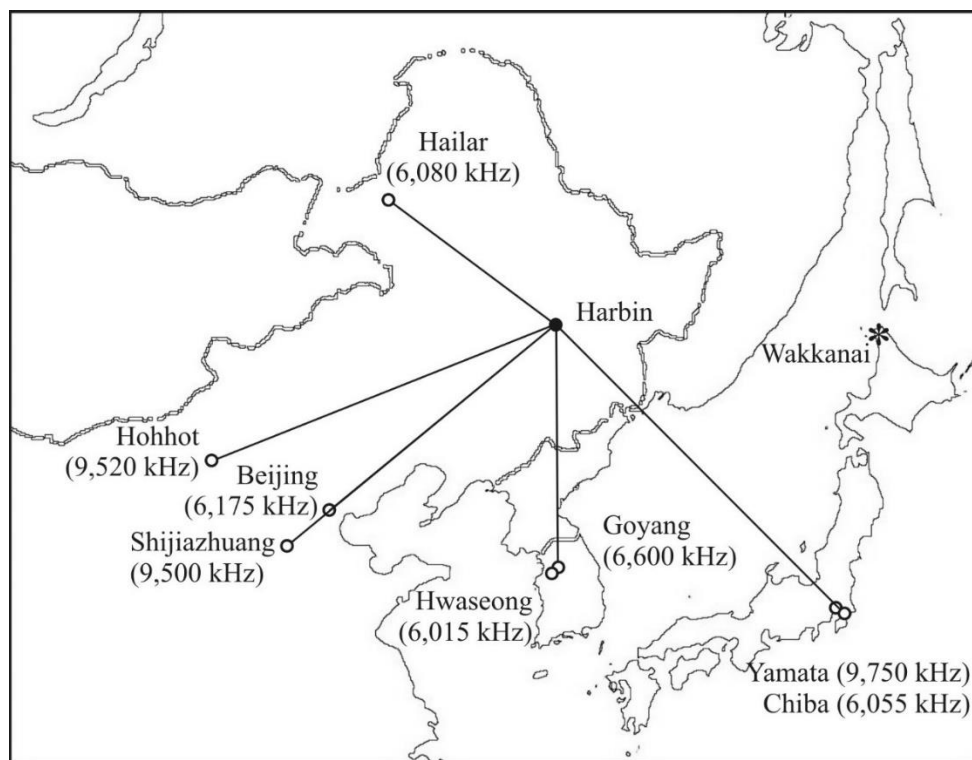
Figure 5: Layout of the propagation paths used for monitoring dynamic processes operating in the ionosphere.

Table 1. Basic Information on Radio-Wave Paths. The data are retrieved from https://fmscan.org/index.php.

Frequency (kHz)	Transmitter coordinates	Location (Country)	Distance to Harbin (km)	Path midpoint coordinates
6,015	37.21°N, 126.78°E	Hwaseong (Korea)	950	41.50°N, 126.73°E
6,055	35.47°N, 140.21°E	Chiba/Nagara (Japan)	1,610	40.63°N, 133.45°E
6,080	49.18°N, 119.72°E	Hailar/Nanmen (PRC)	645	47.48°N, 123.2°E
6,175	39.75°N, 116.81°E	Beijing (PRC)	1,050	42.77°N, 121.75°E
6,600	37.60°N, 126.85°E	Goyang (Korea)	910	41.69°N, 126.77°E
9,500	38.47°N, 114.13°E	Shijiazhuang (PRC)	1,310	42.13°N, 120.41°E
9,520	40.72°N, 111.55°E	Hohhot (PRC)	1,340	43.25°N, 119.12°E
9,750	36.17°N, 139.82°E	Yamata (Japan)	1,570	40.98°N, 133.25°E
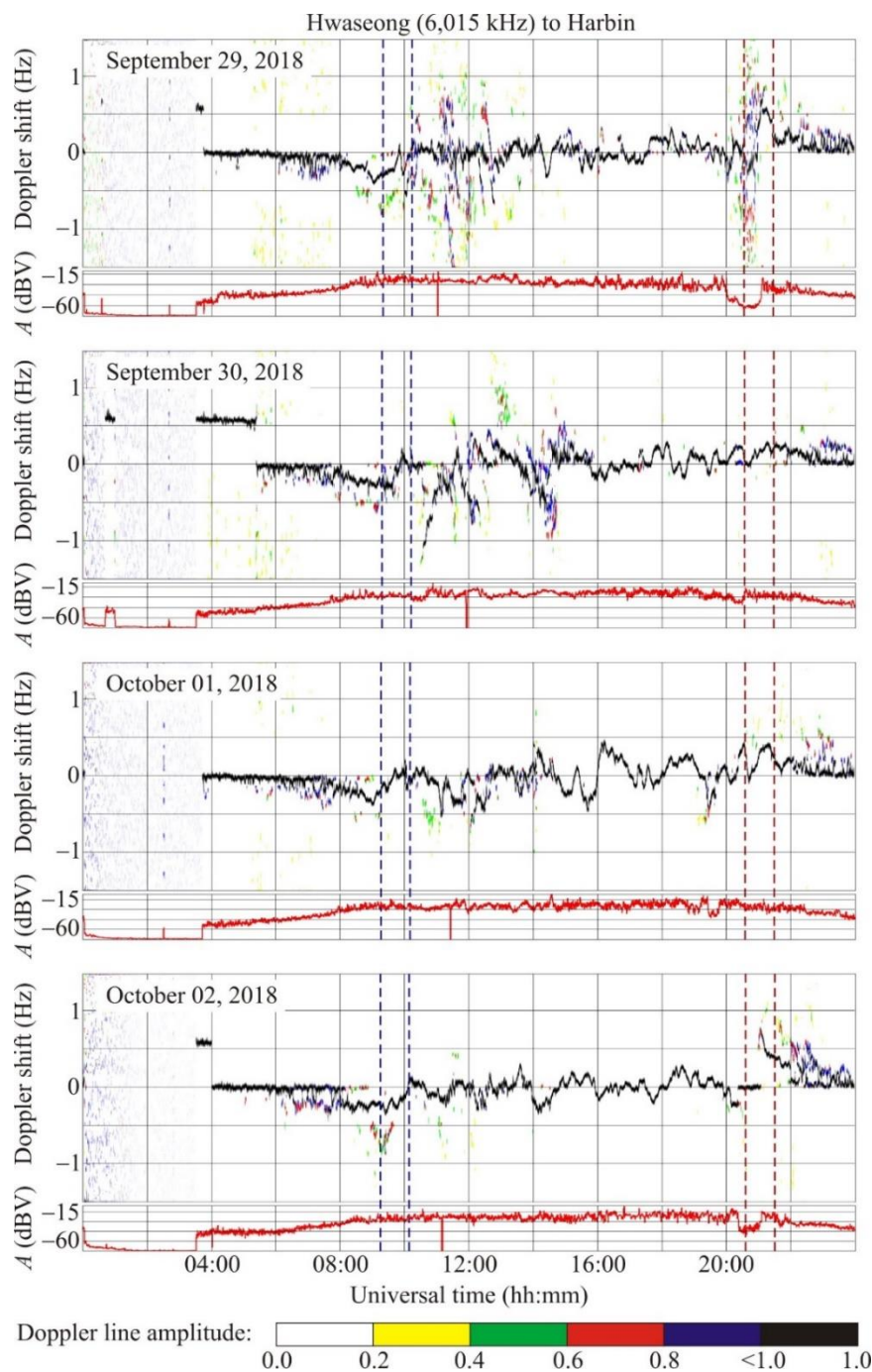
Figure 6: Universal time variations in the Doppler spectra and relative signal amplitude, *A*, along the Hwaseong to Harbin propagation path for the September 29 – October 2, 2018, period. Vertical dashed lines designate instances of sunrise (two right red lines) and sunset (two left blue lines) at the ground and at 100 km altitude. The signal amplitude, *A*, at the receiver output in decibels, dBV (relative to 1 V), is shown below the Doppler spectra in each panel.
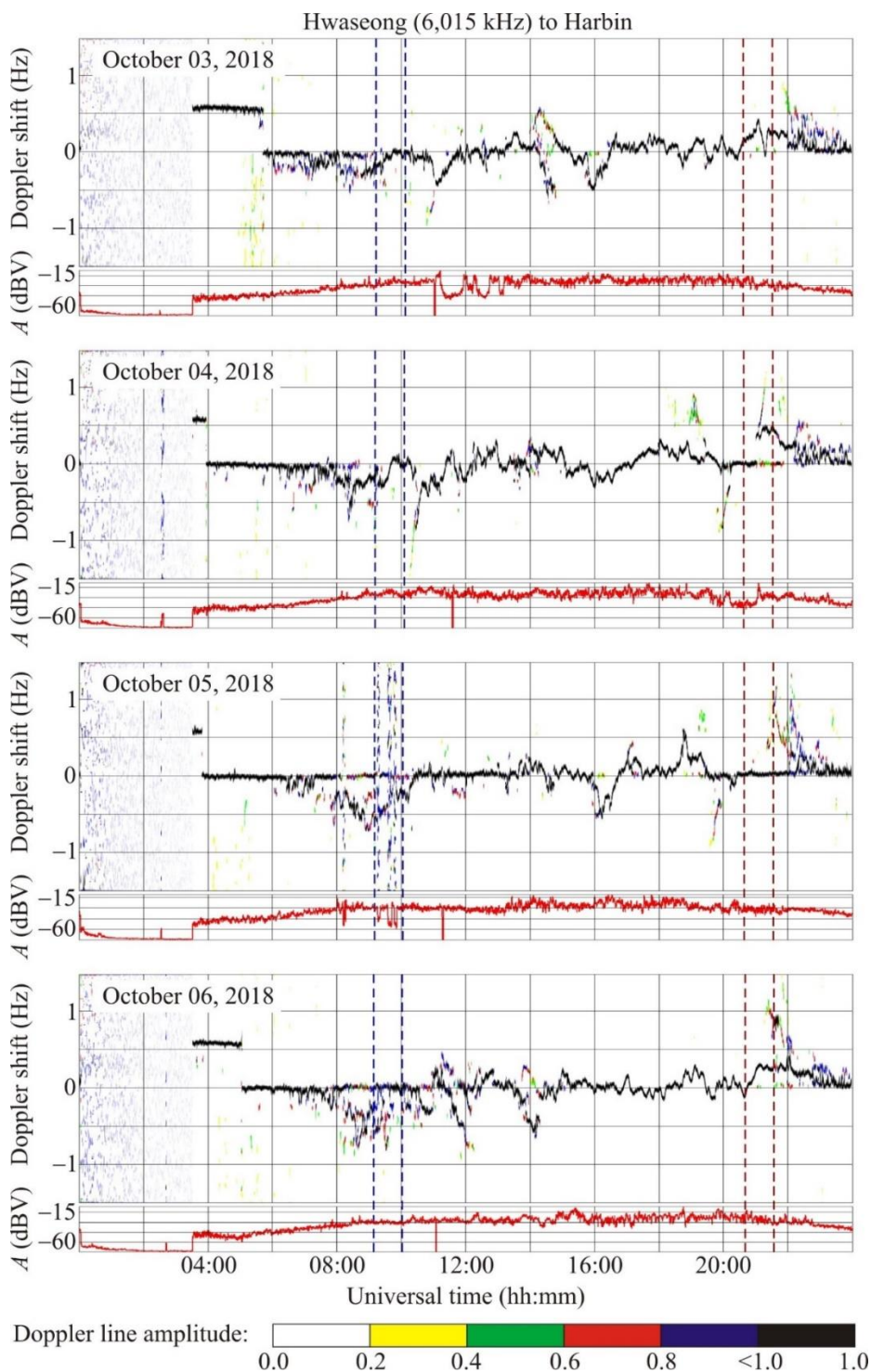
Figure 6: Continued for the October 3–6, 2018 period.

220

6.2 Chiba/Nagara to Harbin radio-wave propagation path

The radio station operating at 6,055 kHz is located in Japan at a great-circle range, R, of ~1,610 km; it was switched off from
225   15:00 UT to 22:00 UT.

Figure 7 shows that on September 29-30, 2018, the Doppler spectra exhibit significant, up to ±1.5 Hz, broadening and such a diffuseness that the main ray is practically not distinguishable. On October 1, 2018, the Doppler shift exhibited ~60-min period, T, quasi-sinusoidal variations with an ~0.3–0.4-Hz amplitude, whereas the signal amplitude, $A(t)$, showed ~30-min period, T, variations with a 5 dBV amplitude. On October 5 and 6, 2018, the quasi-sinusoidal variations were also
230   noted in the Doppler spectra, with ~0.4–0.6-Hz amplitudes, f_{Da}, and with ~60-min and 120-min periods, T. On October 6, 2018, the signal amplitude exhibited ~30- and ~60-min period, T, quasi-sinusoidal variations with a ~5-dBV amplitude.

6.3 Hailar to Harbin Radio-Wave Propagation Path

This transmitter operating at 6,080 kHz is located in the PRC at a great-circle range, R, of 646 km; the transmissions were absent from 02:30 UT to 09:30 UT, whereas the observations of ionospheric dynamics were made impossible during the
235   14:30–20:00 UT period.

The variations in the Doppler spectra and the Doppler shift during the course of the reference days and October 1–2, were practically undistinguishable (Figure 8).

6.4 Beijing to Harbin radio-wave propagation path

This radio station operated at 6,175 kHz in the PRC at a great-circle range, R, of ~1,050 km from the receiver. The
240   transmitter was switched off during 00:00 UT to 09:00 UT and from 18:00 UT to 20:00 UT periods.

On the reference day September 29, 2018, as well as on the next day, the Doppler shift showed small variations ~0.1 Hz (Figure 9), which exhibited increases of up to 0.3–0.5 Hz only over separate time intervals. On October 1, 2018, the Doppler shift exhibited quite ordered variations, with ~30-min and ~110-min period, T, oscillations, and amplitudes, f_{Da}, attaining 0.5 Hz. On October 2, 2018, the amplitude f_{Da} decreased to 0.3 Hz, whereas the periods were observed to vary from
245   20 min to 110 min.

On October 3, 4, and 6, 2018, the Doppler shift exhibited quasi-sinusoidal variations with periods, T, in the 20-min to 90-min range and with 0.1–0.2-Hz amplitudes, f_{Da}.

After 14:00 UT on October 5, 2018, the Doppler shift amplitude, f_{Da}, was observed to increase to 0.2–0.4 Hz and to exhibit periods, T, in the range from 20 min to 80 min.
250   The signal amplitude exhibited temporal variability within the 10 dBV limits.
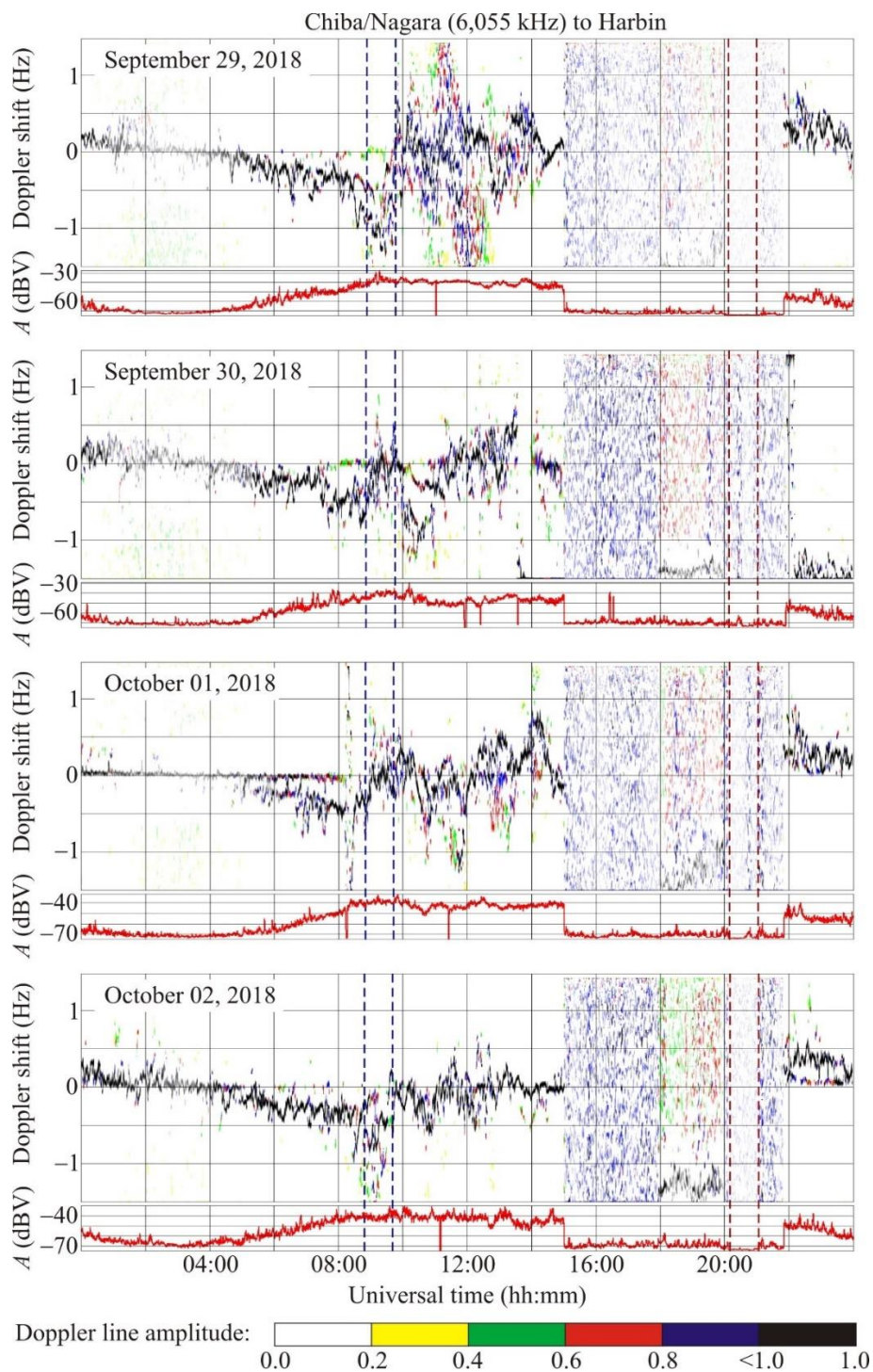
Figure 7: The same as in Figure 6 but for the Chiba/Nagara to Harbin radio-wave propagation path at 6,055 kHz for the September 29 – October 2, 2018, period.
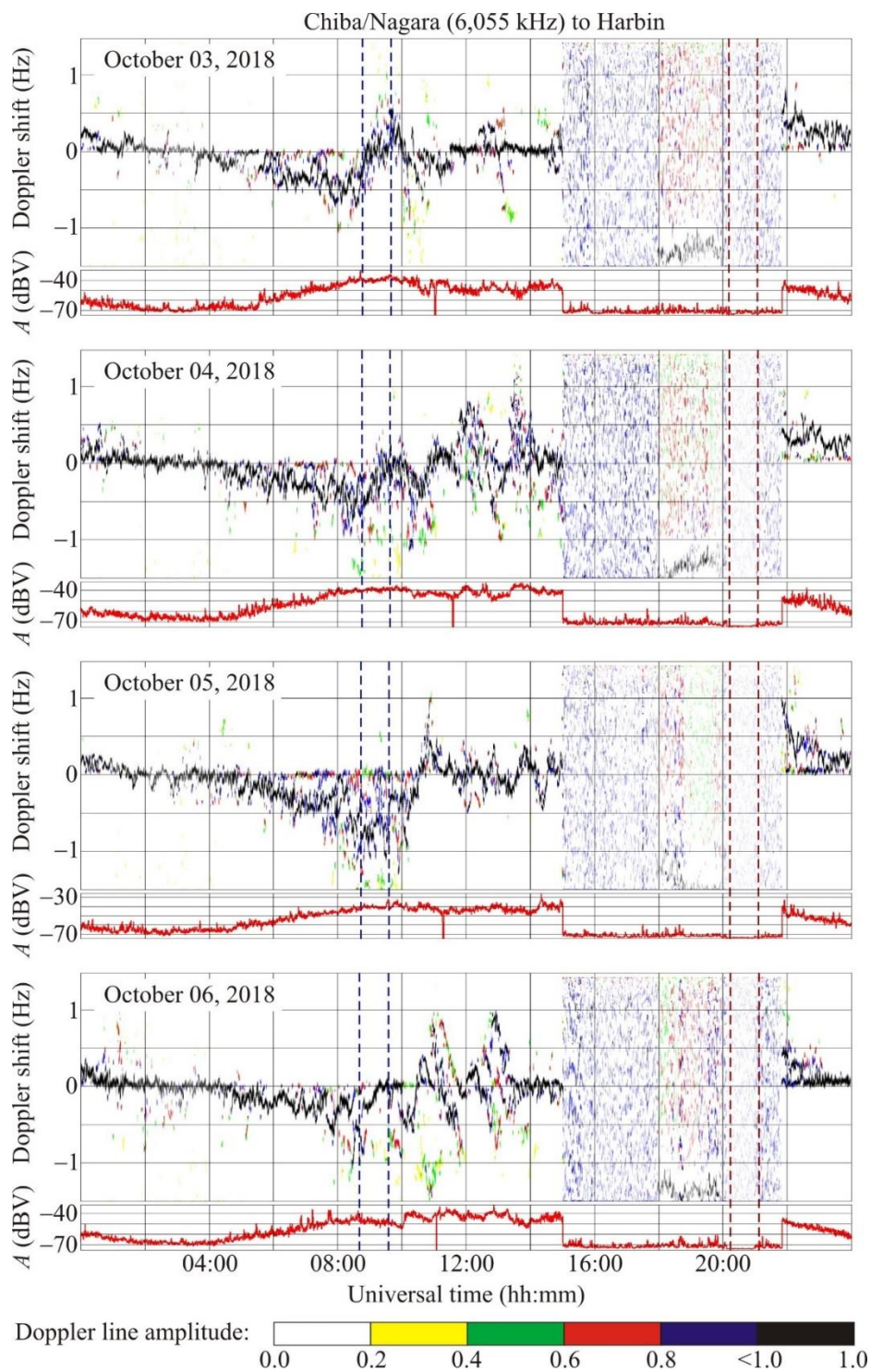
Figure 7: Continued for the October 3–6, 2018 period.
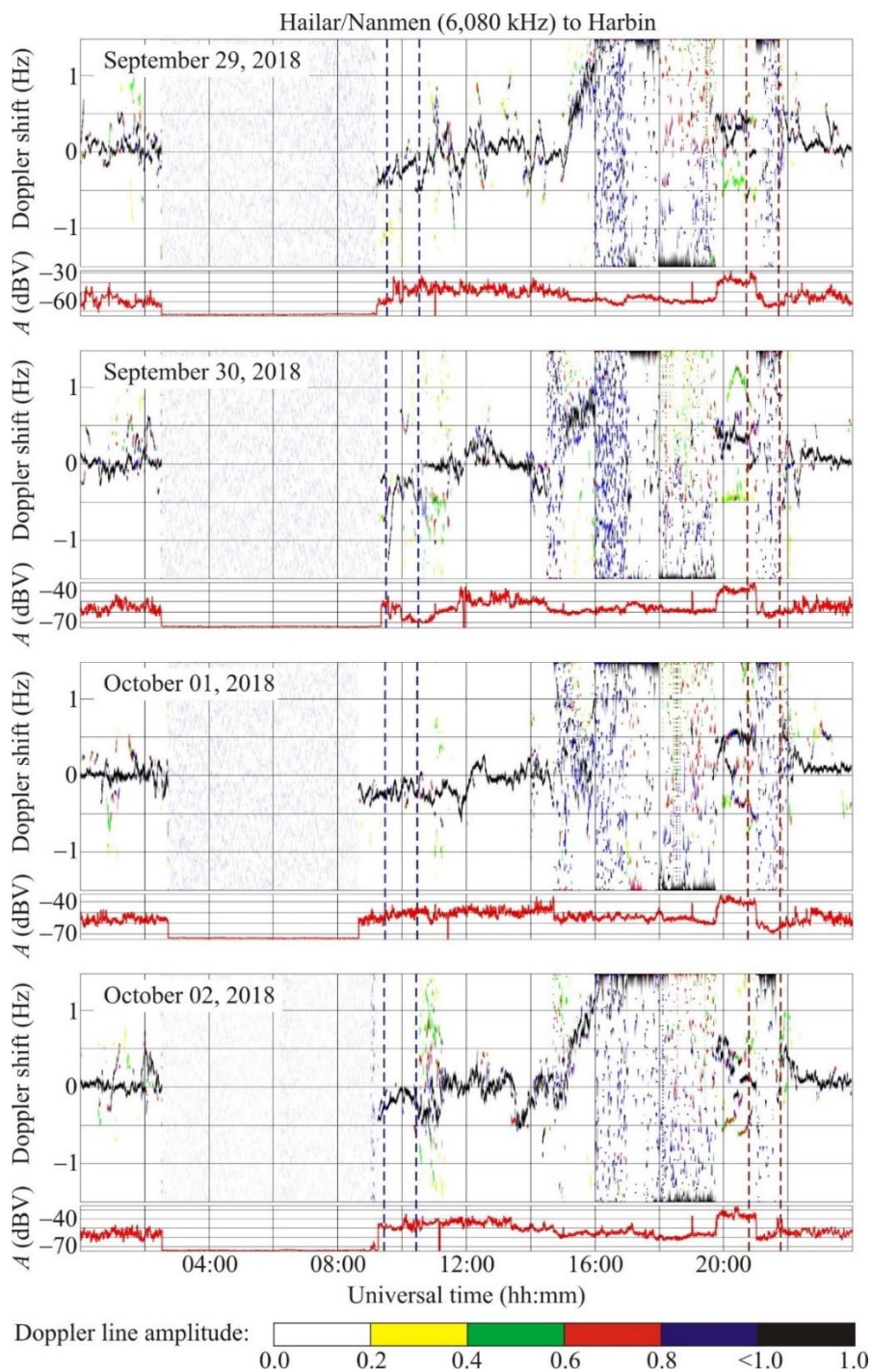
Figure 8: The same as in Figure 6 but for the Hailar to Harbin radio-wave propagation path at 6,080 kHz for the September 29 – October 2, 2018, period.
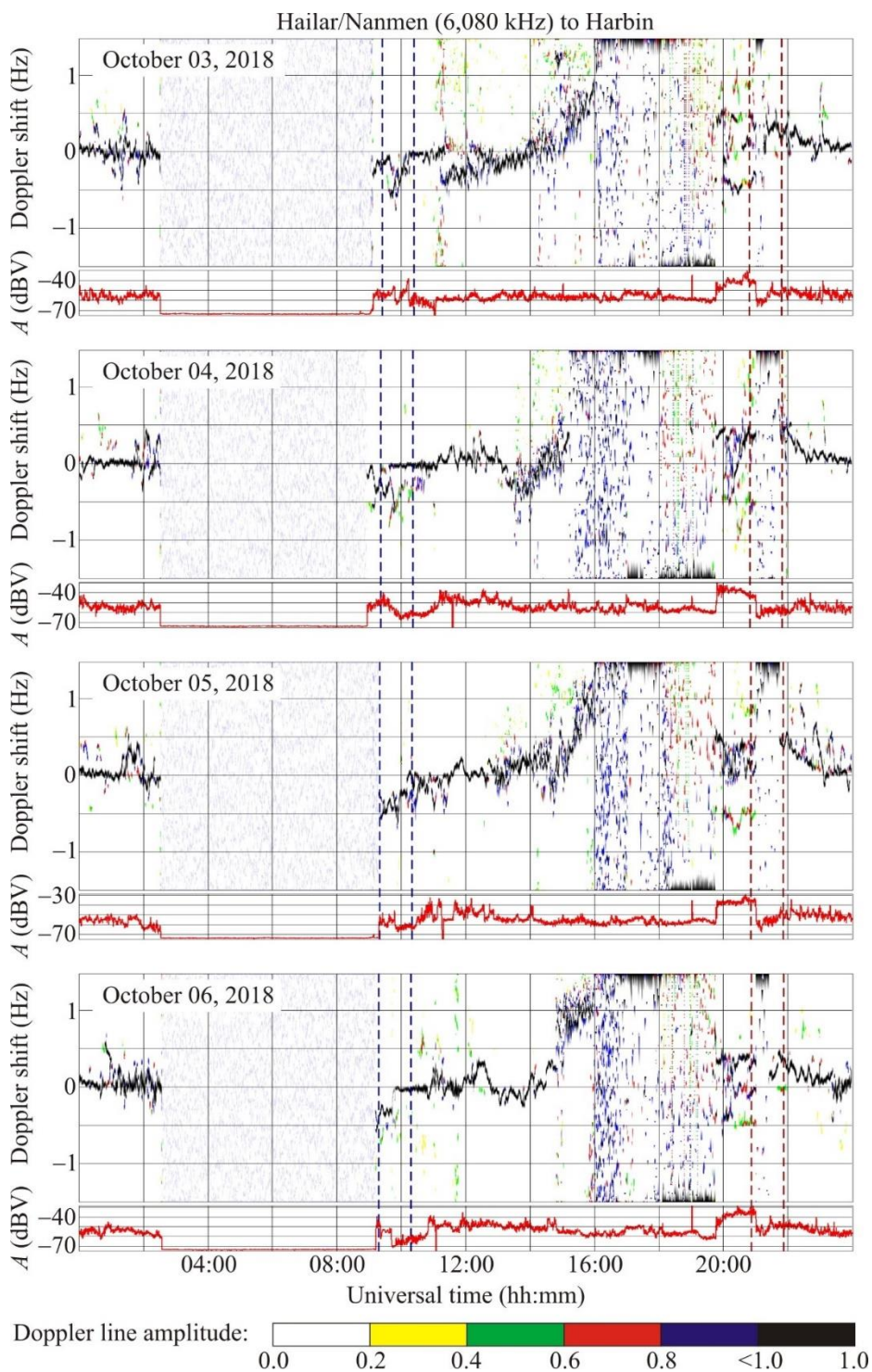
Figure 8: Continued for the October 3–6, 2018 period.
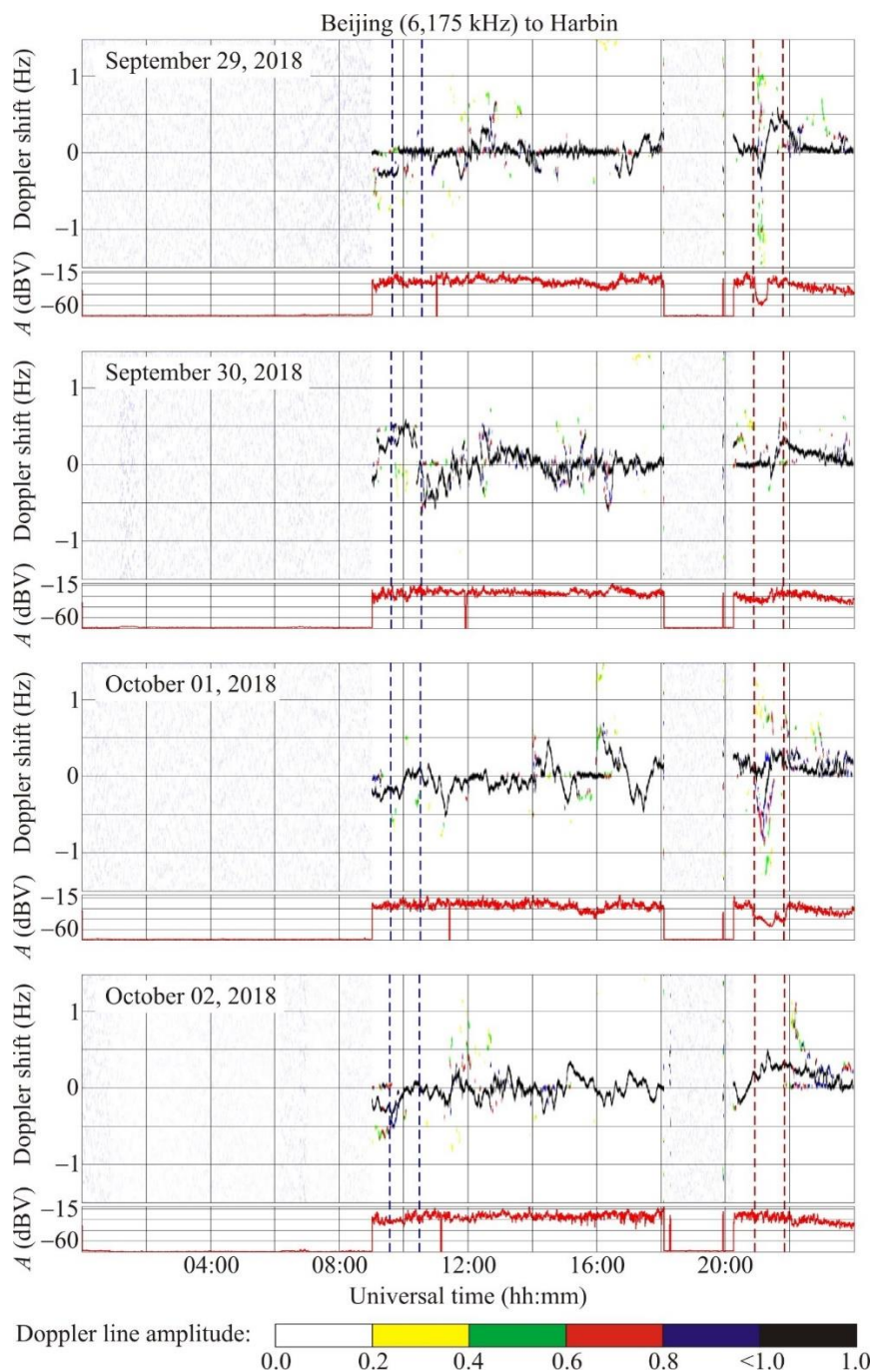
Figure 9: The same as in Figure 6 but for the Beijing to Harbin radio-wave propagation path at 6,175 kHz for the September 29 – October 2, 2018, period.

265
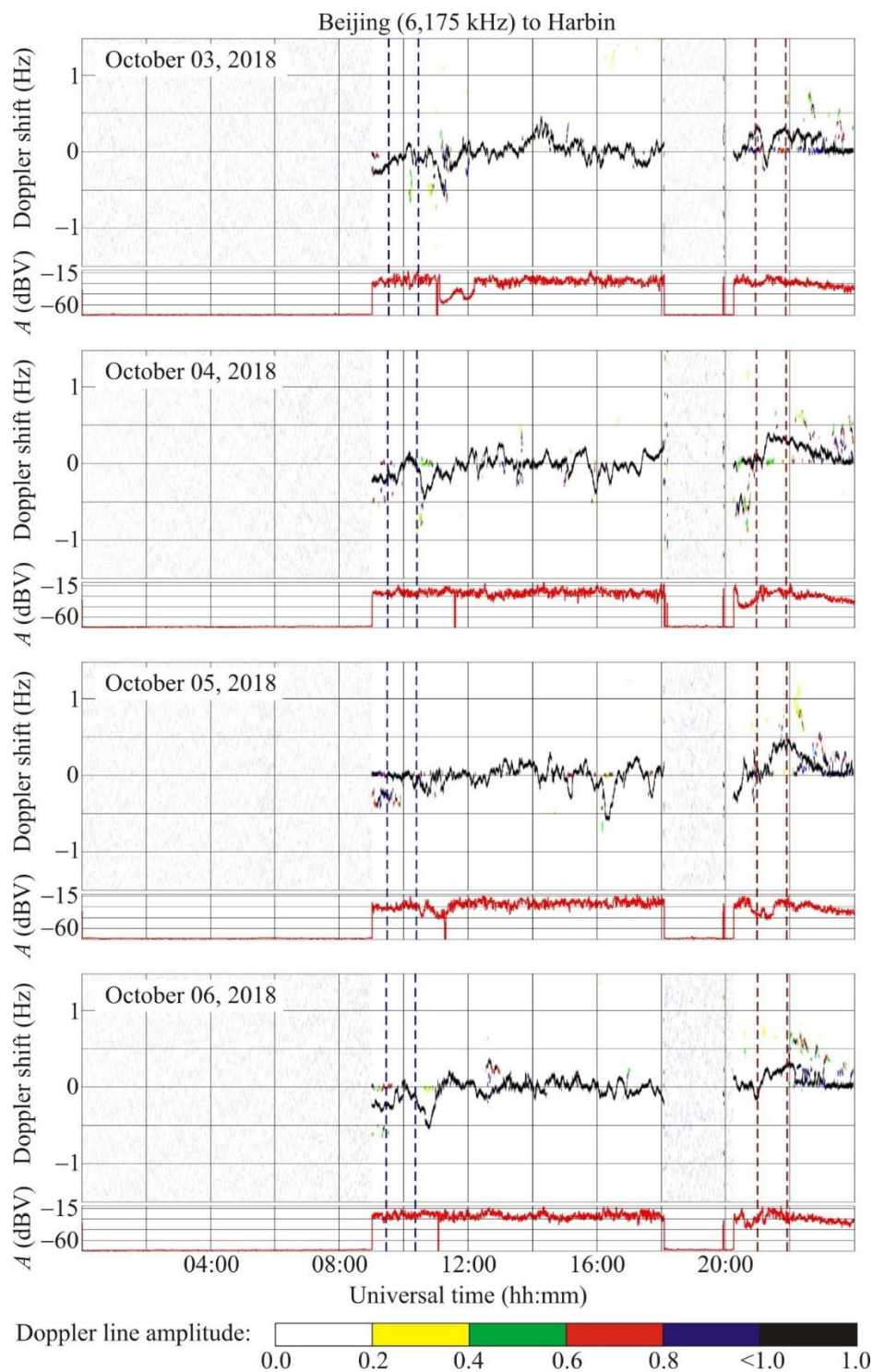
Figure 9: Continued for the October 3–6, 2018 period.

6.5 Goyang to Harbin radio-wave propagation path

This transmitter operating at 6,600 kHz is located in the Republic of Korea at a great-circle range of ~910 km from the receiver; it was switch off from 00:00 UT to 05:00 UT and from 22:20 UT to 24:00 UT.

On the reference day September 29, 2018, the Doppler shift showed fluctuations within the ±(0.2–0.3) Hz limits (Figure 10). The next day, the Doppler spectrum broadening was observed to occur from 12:00 UT to 16:00 UT whereas the Doppler shift exhibited quasi-sinusoidal ~20–24-min period, T, 0.1–0.2-Hz amplitude, f_{Da}, variations.

The Doppler ±0.6 Hz spectrum broadening was observed to occur on October 1, 2018, while the Doppler spectra exhibited ~20–120-min period, T, ~0.1–0.7-Hz amplitude, f_{Da}, variations; considerable, up to 20 dBV, variations were noted in the signal amplitude.

On October 2, 2018, the Doppler shift exhibited significant, ±(0.2–0.3) Hz, variations, with a quasi-period, T, of 24 min and amplitude, f_{Da}, of ~0.2 Hz. Considerable fluctuations in the Doppler spectra, the Doppler shift, and in the signal amplitude were noted on October 3, 2018. On October 4, 2018, from 14:00 UT to 20:00 UT, the Doppler shift showed changes within the –0.3 Hz to 0.3 Hz limits, the quasi-sinusoidal processes were expressed weakly, and the signal amplitude fluctuated wildly, by 30 dBV. On October 5, 2018, the variations in the Doppler shift did not exceed ±0.2 Hz, the fluctuations in the signal amplitude were also insignificant. The Doppler shift was observed to increase up to ±(0.3–0.5) Hz during the October 6, 2018 11:00–14:00 UT period, whereas from 15:00 UT to 18:00 UT, the quasi-sinusoidal oscillations in the Doppler shift were observed to occur with a ~20-min period, T, and ~0.1-Hz amplitude, f_{Da}, while quasi-sinusoidal variations in the signal amplitude, $A(t)$, were observed to occur with a ~55–80-min period, T, and ~7–8 dBV amplitude.

6.6 Shijiazhuang to Harbin radio-wave propagation path

This radio station operating at 9,500 kHz is located in the PRC at a great-circle range, R, of ~1,310 km from the receiver.

Figure 11 shows that the value of the Doppler shift, $f_D(t)$, was close to zero on each night. The Doppler shift was observed to be negative, attaining a minimum of –(0.20–0.25) Hz, two to three hours before the sunset at the ground. During the night of September 29, 2018, the signal amplitude was observed to fluctuate wildly within the 20 dBV limits and to be accompanied by fluctuations in the Doppler shift. A second ray shifted by –0.5 Hz with respect to the main ray was observed to appear during the 16:00–20:00 UT period. From September 30, 2018, through October 6, 2018, nighttime, the signal frequency approached the maximum usable frequency and ionospheric signal was about to penetrate the ionosphere, which resulted in a 10–20 dBV decrease in the signal amplitude, whereas the Doppler spectra became low informative. These circumstances have significantly hampered the search for the ionospheric response to the super typhoon action. Nevertheless, the Doppler shift exhibited considerable, attaining –1 Hz, variations on October 1, 2018. Significant variations in the Doppler shift were noted at the beginning of the October 2, 2018, night and after midnight on October 3, 4, 5, and 6, 2018; in particular, the ray shifted by –0.5 Hz was observed to occur.
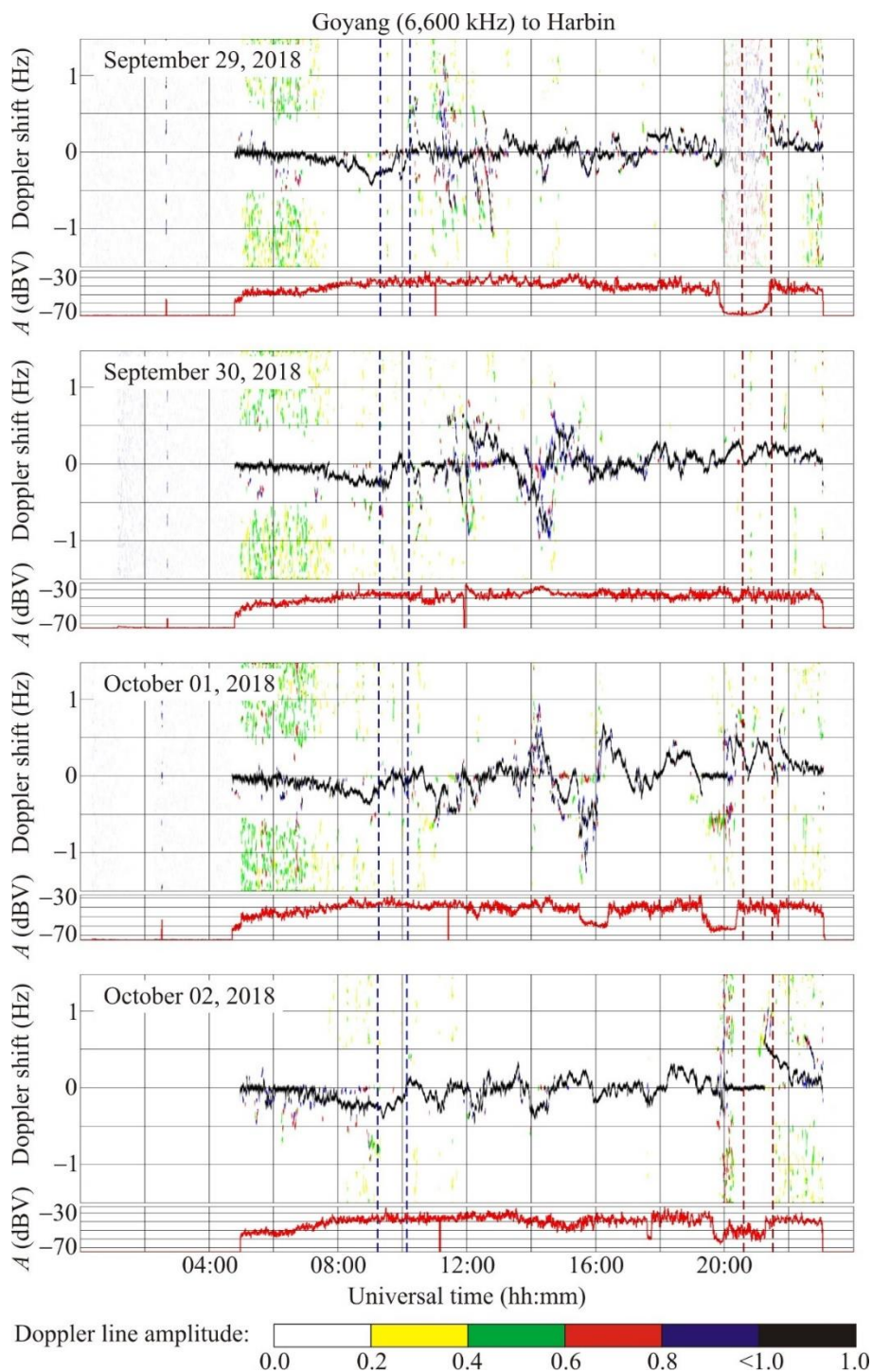
Figure 10: The same as in Figure 6 but for the Goyang to Harbin radio-wave propagation path at 6,600 kHz for the September 29 – October 2, 2018, period.

305
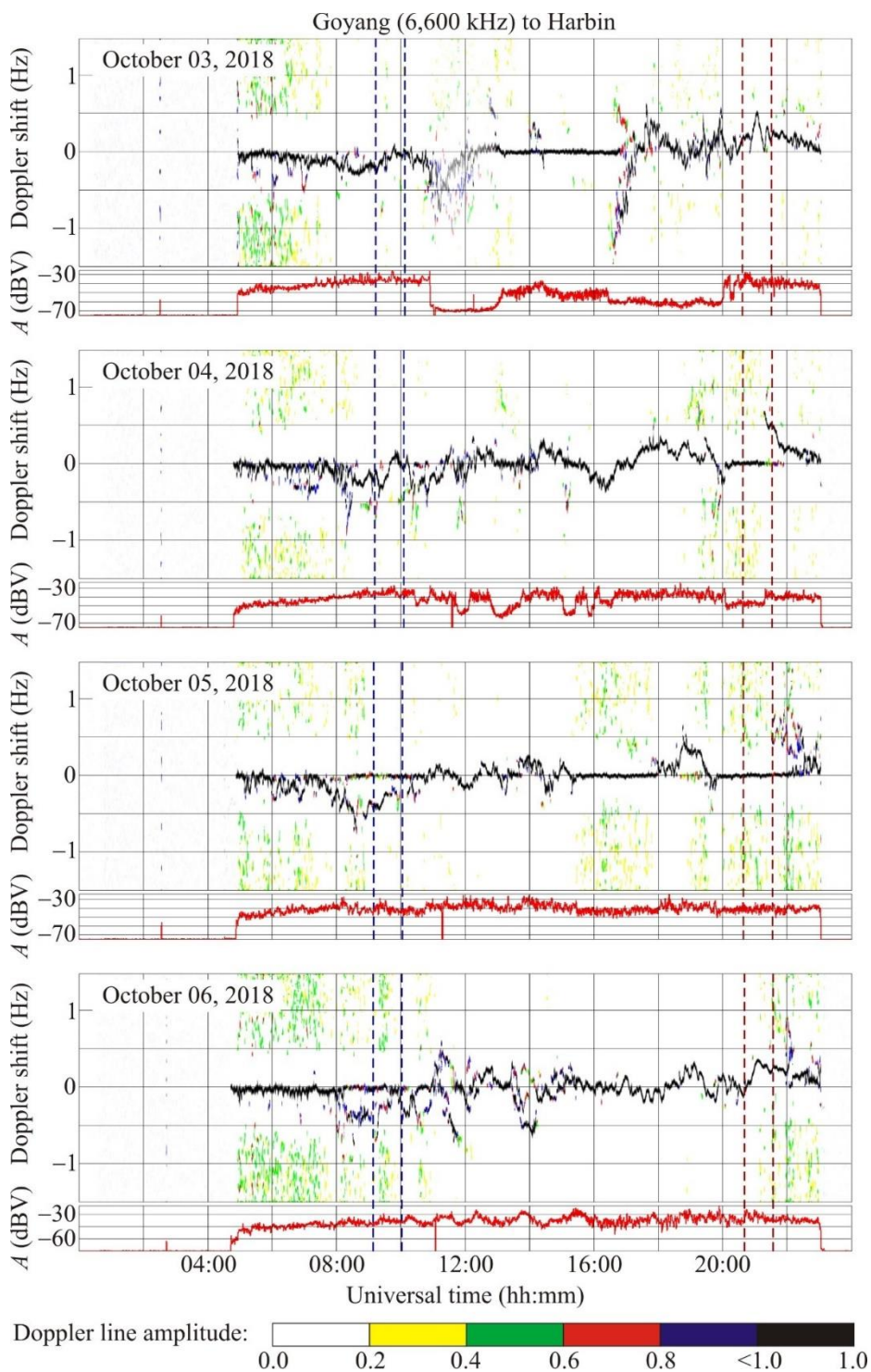
310   **Figure 10: Continued for the October 3–6, 2018 period.**
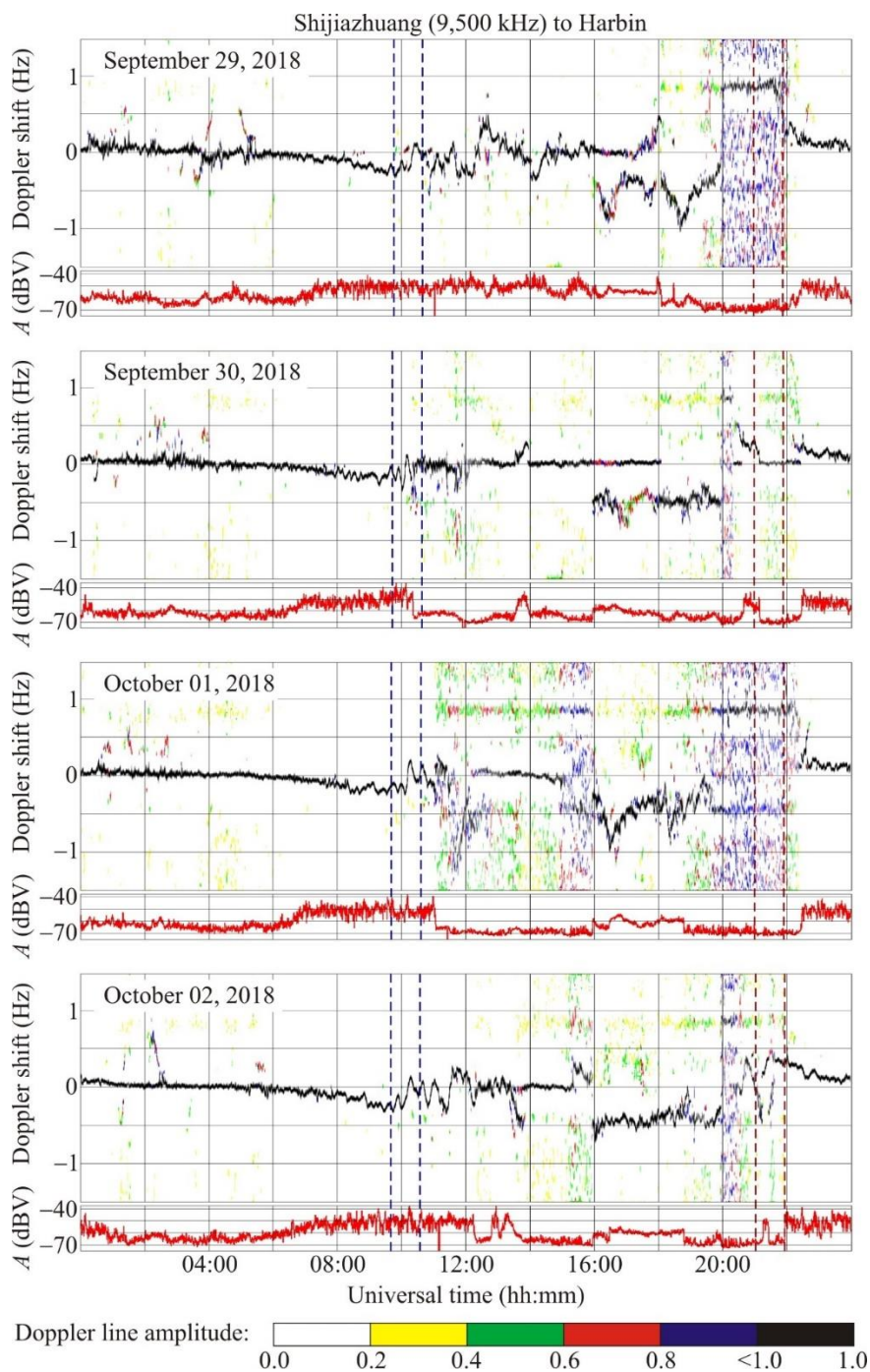
Figure 11: The same as in Figure 6 but for the Shijiazhuang to Harbin radio-wave propagation path at 9,500 kHz for the September 29 – October 2, 2018, period.

315
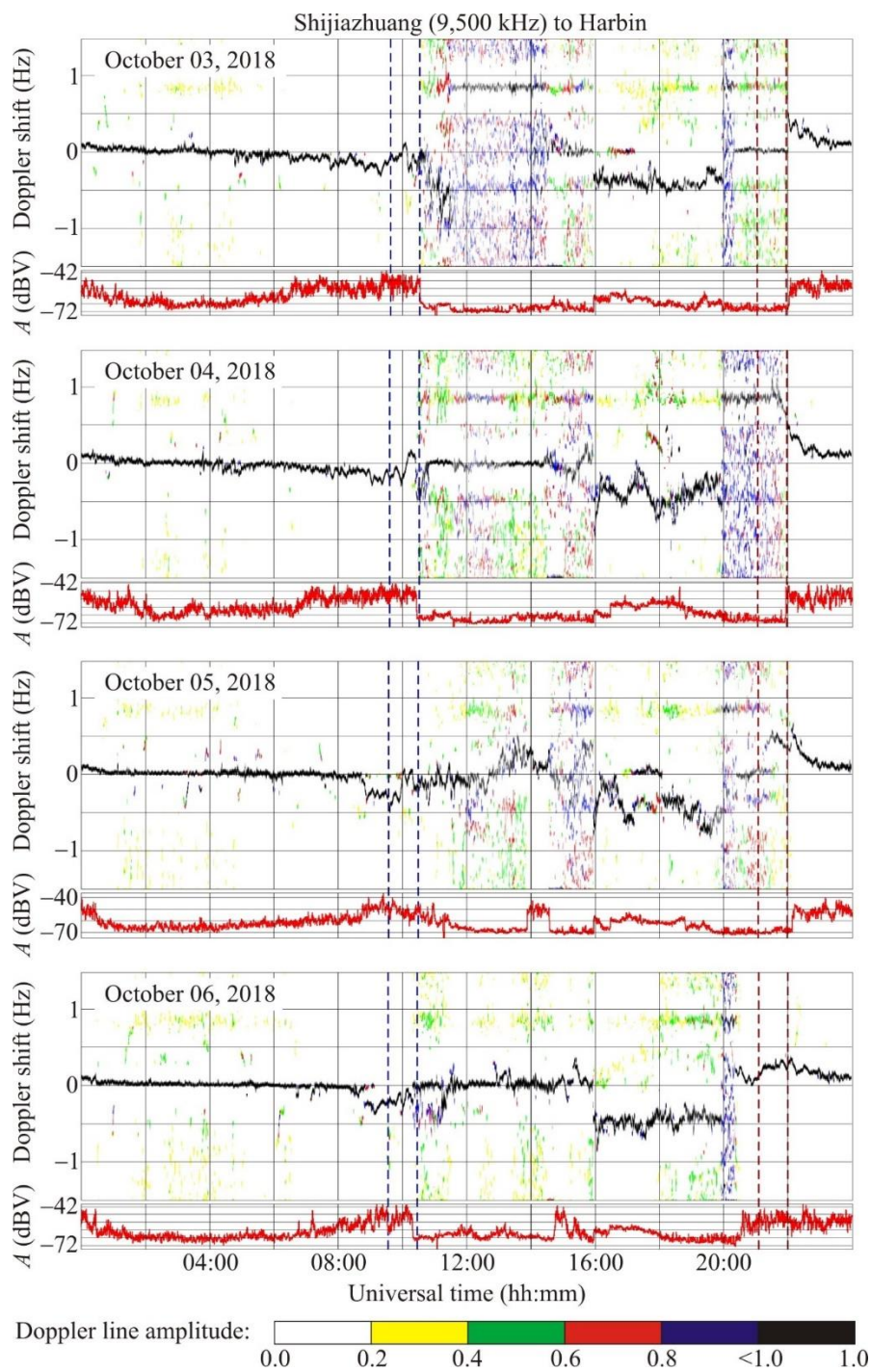
Figure 11: Continued for the October 3–6, 2018 period.

6.7 Hohhot to Harbin radio-wave propagation path

320 This transmitter operating at 9,520 kHz is located in the PRC at a great-circle rang, R, of ~1,340 km; it was switched off from 16:00 UT to ~22:00 UT.

      The frequency of this radio wave became greater than the maximum usable frequency and the radio wave penetrated the ionosphere during the second half of the nights. Consequently, the observation of became impossible. The Doppler spectra exhibited substantial variations (±0.5 Hz) on September 29, 2018, from 12:00 UT to 16:00 UT (Figure 12).

325 During the night of September 30, 2018, the reflection of radio waves took place from the sporadic E layer, resulting in $f_D(t) \approx 0$ Hz. During October 1, 2018, nighttime, the Doppler shift $f_D(t) \approx 0$ Hz as well. During the course of the October 2, 2018, night, the Doppler shift was observed to change from –0.3 Hz to 0.3 Hz, the signal amplitude was observed to exhibit considerable variability, up to 20 dBV, In the course of the October 3–6, 2018 nights, the measurements were ineffective, whereas $f_D(t) \approx 0$ Hz at daytime.

6.8 Yamata to Harbin radio-wave propagation path

330

This radio station operating at 9,750 kHz is located in Japan at a great-circle range, R, of ~1,570 km. The transmitter was switch off from 16:00 UT to ~22:00 UT.

      A characteristic feature of these observations is that two signals were received, the Doppler shift of which were shifted by 1 Hz from September 29, 2018, through October 3, 2018 and by 0.5 Hz from October 4, 2018 through October 6,

335 2018, as can be seen in Figure 13.

      During all the days, the Doppler shift exhibited insignificant variations at daytime, whereas in the evening it became negative. The Doppler shift and the Doppler spectrum variations were observed to be significant (from –1 Hz to 1 Hz) on September 29 and 30, 2018. On October 1, 2018, the Doppler spectra exhibited diffuseness, while the signal amplitude $A(t)$ variability was observed to attain 30 dBV. During October 2, 2018 nighttime, the Doppler shift was observed to vary from –

340 0.4 Hz to 0.4 Hz, while the variations in $A(t)$ also attained 30 dBV. The Doppler spectra and the Doppler shift showed insignificant temporal variability on October 3 and 4, 2018; at the same time the signal amplitude exhibited 20–30 dBV variations.

      On October 5 and 6, 2018, the magnitude of the Doppler shift attained ±0.2 Hz, while the signal also exhibited considerable variations in amplitude, up to 30 dBV.

345
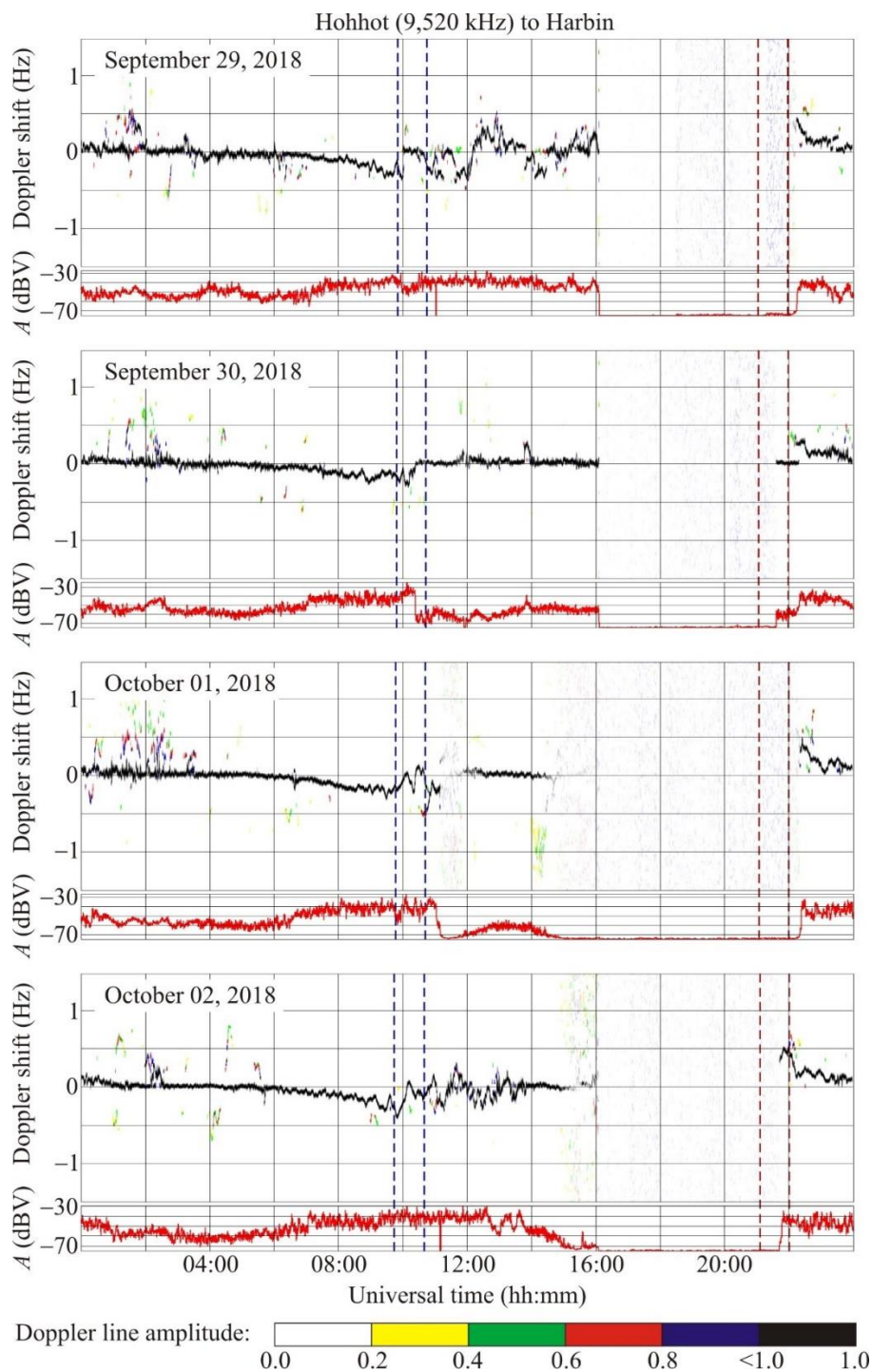
Figure 12: The same as in Figure 6 but for the Hohhot to Harbin radio-wave propagation path at 9,520 kHz for the September 29 – October 2, 2018 period.
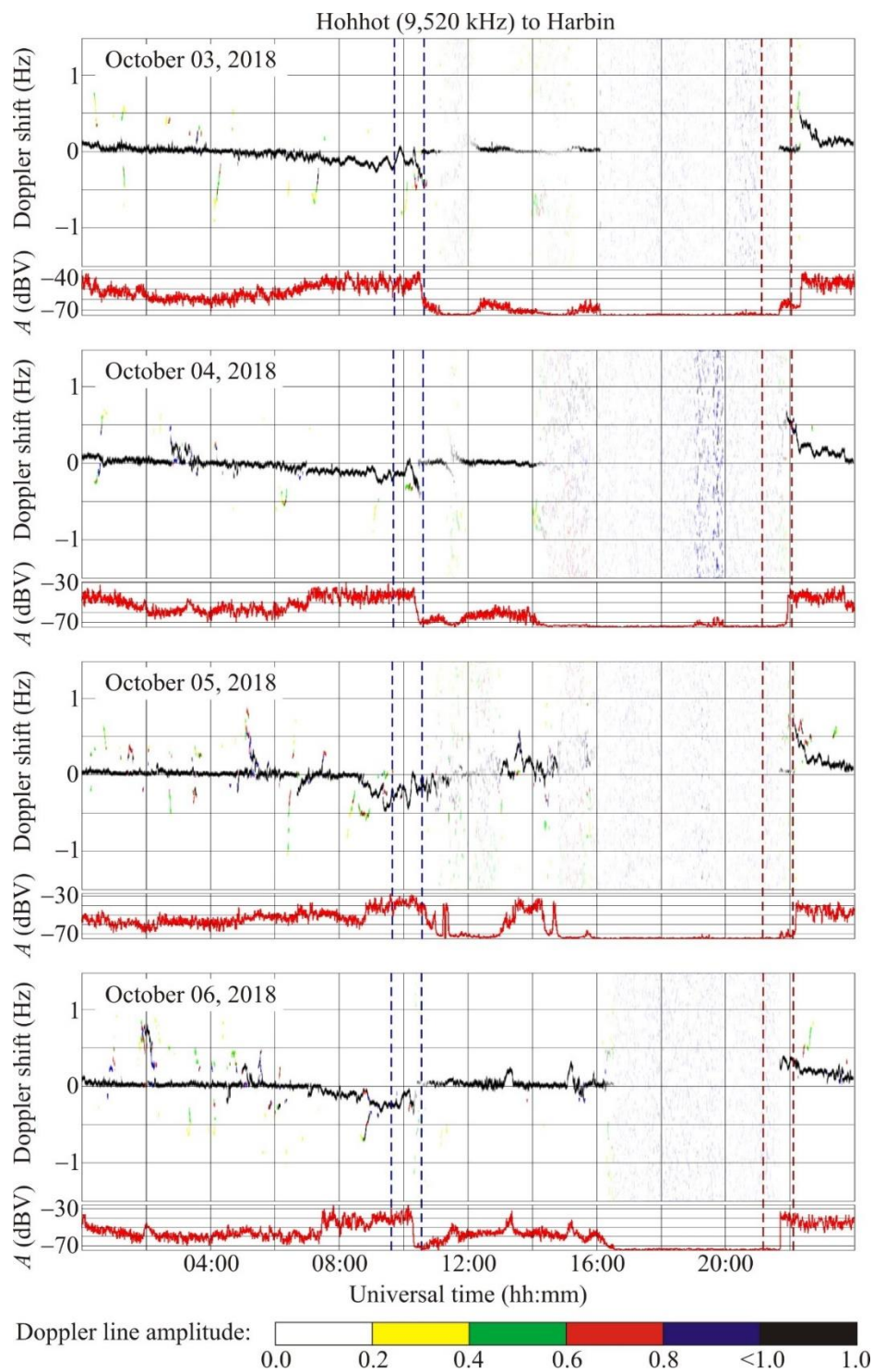
Figure 12: Continued for the October 3–6, 2018 period.
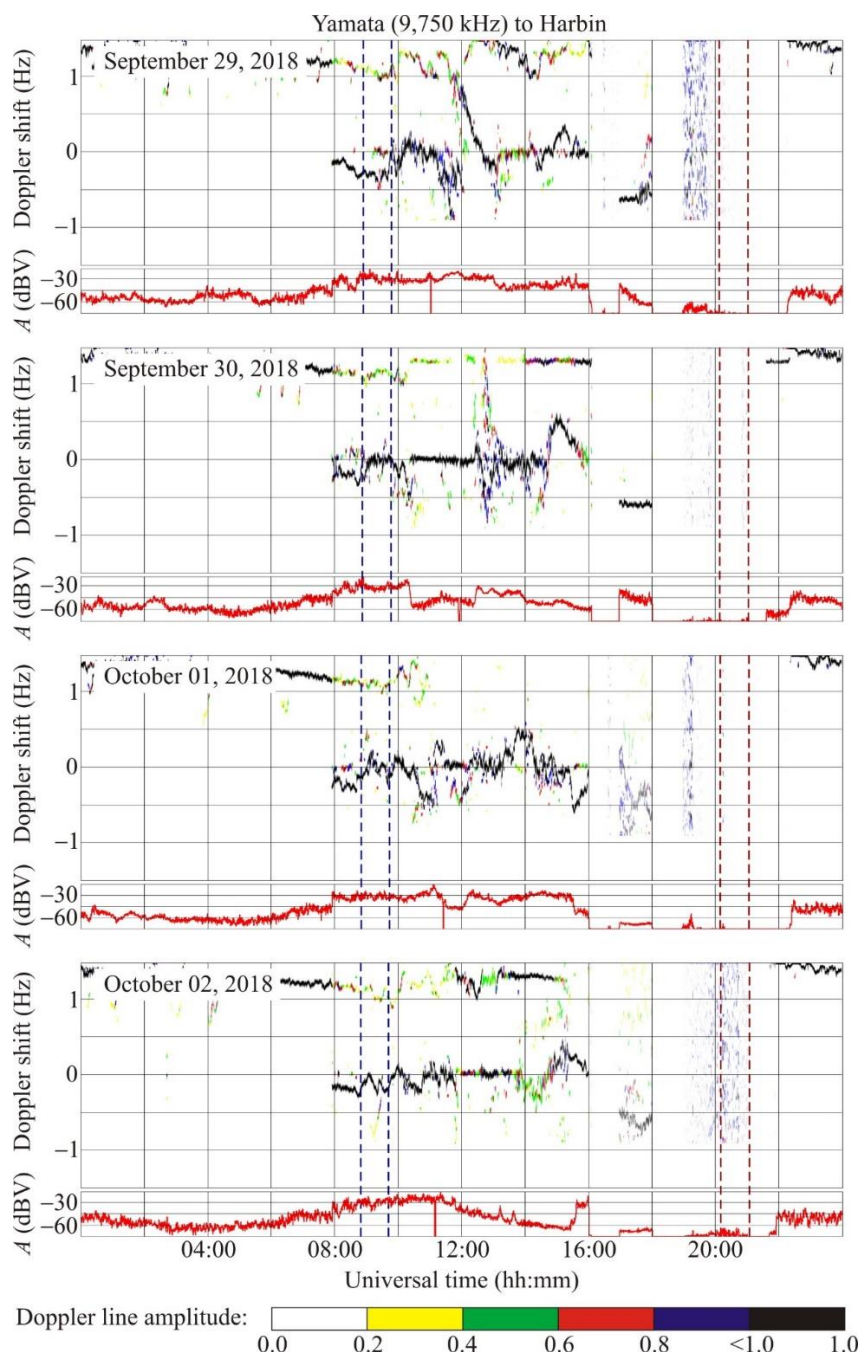
Figure 13: The same as in Figure 6 but for the Yamata to Harbin radio-wave propagation path at 9,750 kHz for the September 29 – October 2, 2018 period.

355
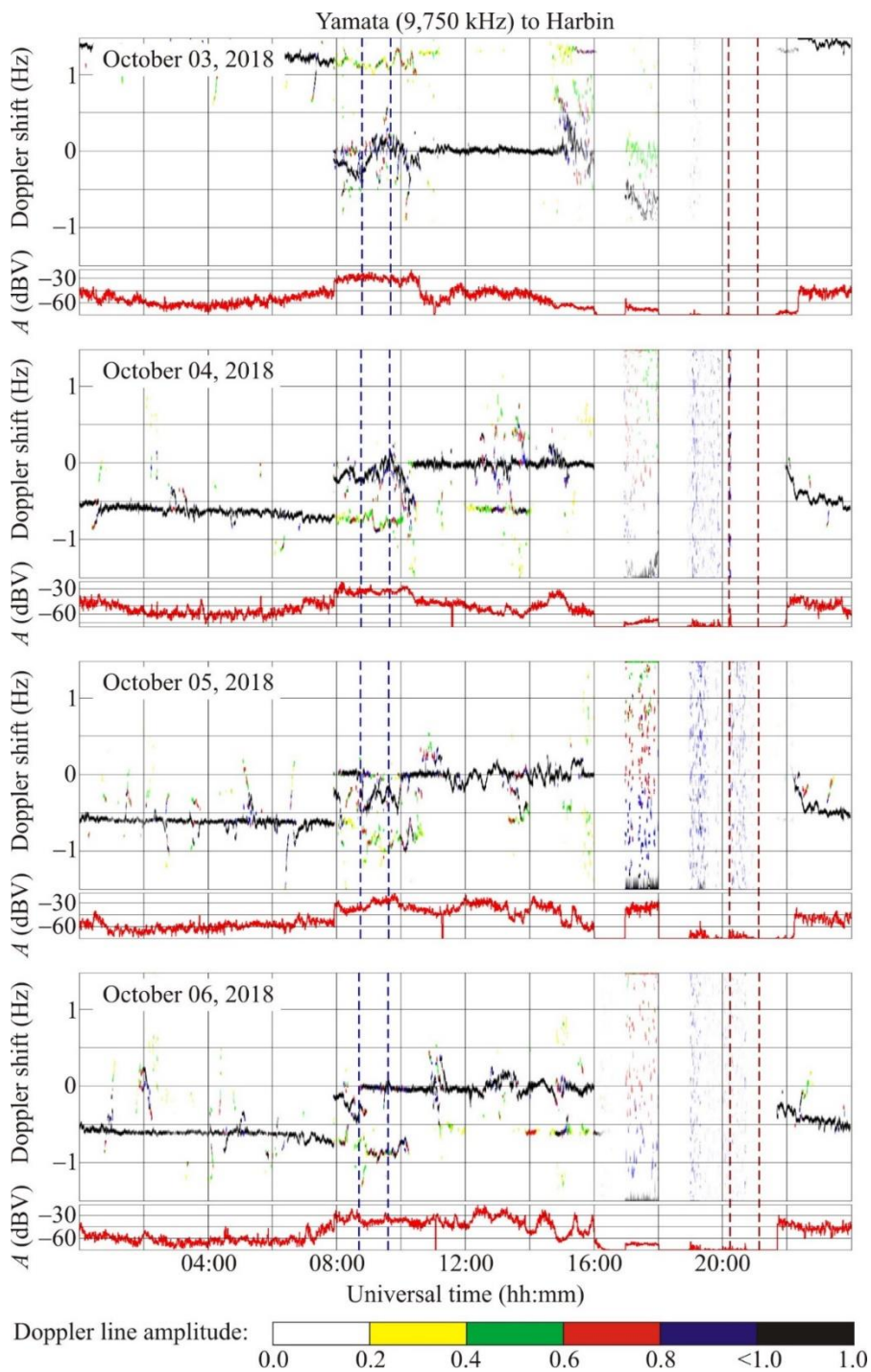
360

Figure 13: Continued for the October 3–6, 2018 period.

7 Discussion

7.1 Ionospheric effects from the super typhoon

365 The Doppler spectra and the Doppler shift observed during sunlit hours exhibited insignificant temporal variability through the course of the typhoon action, since the radio waves in the ~6–10 MHz band were reflected from the ionospheric *E* region or from the sporadic *E*. At night, the radio waves were reflected from the ionospheric *F* region, and the Doppler shift was observed to attain up to 0.5–1 Hz. The temporal variations in the Doppler shift were also generated by the movement of the solar terminator.

370 The diurnal variations of the signal amplitude were observed to attain 30 dBV, and the signal amplitude $A(t)$ at night was three orders of magnitude greater than during the day, which is due to the disappearance of the absorbing *D* region.

The ionospheric effects from the super typhoon Kong-Rey are discussed further below. The super typhoon Kong-Rey's power gained a maximum value during the second half of October 1, 2018. The Doppler shift and the Doppler spectra showed the greatest variations during the October 1, 2018 night, despite the propagation path midpoints were located 375 ~2,800–3,300 km away from the super typhoon. As should be expected, the greatest effects were observed to occur along the propagation paths emanating from the transmitters located closest to the typhoon, i.e., the radio stations Chiba/Nagara, Goyang, and Yamata (Japan) and Hwaseong (Republic of Korea). The ionospheric effects from the super typhoon Kong-Rey were absent along the Hohhot to Harbin radio-wave propagation path located at the farthest range to the typhoon on October 1, 2018.

380 On October 2, 2018, the super typhoon Kong-Rey approached ~600 km off the propagation path midpoints, and its power reduced by a factor of 2 by night. As a result, the ionospheric response to the typhoon action also reduced noticeably.

The ionospheric effects were either weak or absent during the daytime of October 2, 2018 and on October 3 and 4, 2018. An increase in the amplitude of the Doppler shift and, partly, in the signal amplitude variations were observed to occur on October 5, 2018, as well as along a number of propagation paths on October 6, 2018. During the October 5 and 6, 2018 385 nights, the typhoon was located at a range of ~1000–1500 km from the propagation path midpoints, and its power was reduced by a factor of ~3, as compared to that observed on October 1, 2018.

7.2 Wavelike disturbances

Wavelike disturbances in the ionosphere were also observed to occur on the reference days of September 29 and 30, 2018. The amplitude of the Doppler shift was observed to noticeably (factor of ~2–3) increase on October 1–2 and 5–6, 2018. In a 390 number of cases, variations in the signal amplitude were observed to increase as well. Based on the periods (from 20 min to 120 min), the wavelike disturbances in the ionosphere are caused by atmospheric gravity waves (Gossard and Hooke, 1975).

Given known f_{Da} and T, the amplitude, δ_{Na}, of quasi-sinusoidal variations in the electron density can be estimated on a relative scale. To do this, one can use the following equation (Chernogor et al., 2020; Guo et al., 2020):

$$\delta_{Na} = \frac{K}{4\pi} \frac{cT}{L} \frac{f_{Da}}{f}, \tag{1}$$

395 where

$$K = \frac{1 + \cos\theta}{2\left(1 + 2\xi\tan^2\theta\right)\cos^2\theta} \; ; \; \xi = \frac{z_r - z_0}{r_0} \; ; \; \tan\theta = \frac{R}{2z_r}, \tag{2}$$

c is the speed of light, θ is the angle of incidence with respect to the vertical at the basis of the ionosphere, z_0 is the altitude of the beginning of the layer giving a contribution to the Doppler shift, z_r is the altitude of reflection, r_0 is the mean Earth's radius, L is the thickness of the atmospheric region giving a contribution to the Doppler shift.

400   Substituting $T \approx 20$ min and $f_{Da} \approx 0.1$ Hz in (1) and taking into account (2) yield $\delta_{Na} \approx 0.4\%$. If $T \approx 30$ min and $f_{Da} \approx 0.2$ Hz, then $\delta_{Na} \approx 1.2\%$. Also, $T \approx 60$ min and $f_{Da} \approx 0.5$ Hz give $\delta_{Na} \approx 6\%$.

       Thus, the super typhoon action in the ionosphere leads to an increase in the amplitude of variations in the electron density, depending on the period of quasi-sinusoidal disturbances, by units to several tens of per cent.

       In addition, the amplitude of quasi-sinusoidal variations is observed to increase in the Doppler shift along many
405 propagation paths under the super typhoon action in the course of the movement of the solar terminator. Such an effect during the dawn terminator is not observed reliably.

       Consequently, the synergistic action of the dusk terminator and typhoons takes place on the ionosphere. An effect analogous to the one described above was observed earlier by Edemsky and Yasyukevich (2018) who made use of GPS technology for probing the wave disturbances.

410 **7.3 Comparison of ionospheric effects from typhoons**

A multifrequency multiple path coherent software defined radio system developed at the Harbin Engineering University has been in routine use for several years for the determination of variations in radio wave characteristics in the 5–10 MHz band and in ionospheric parameters, which accompanied the movement of the super typhoon Hagibis (Chernogor et al., 2021), Ling-Ling and Faxai (Chernogor et al., 2022), Lekima, Kong-Rey, et al. The response of the ionosphere to typhoon action
415 has been shown to be dependent not only on the parameters of typhoons, but also on the state of atmospheric and space weather, local time, and on other geophysical parameters. Not only are common manifestations in the response found, but also individual manifestations that are characteristic of the given super typhoon. The common manifestations include: (1) the aperiodic (chaotic) character of the ionospheric response; (2) the magnitude of the response shows an apparent abatement with increasing distance between the typhoon and the propagation path midpoints; (3) the response exhibits a maximum with
420 distance between the typhoon and the propagation path midpoints approaching a minimum; (4) Doppler shift spectrum broadening up to ±1 Hz due to an increase in the number of rays; (5) the occurrence of quasi-sinusoidal variations in the Doppler shift with amplitudes of ~0.1–0.5 Hz and periods of 2–5 min and 10–100 min; (6) the generation or enhancement of infrasound (periods $T \approx 2$–5 min) and atmospheric gravity waves (periods $T \approx 10$–100 min); (7) disturbances of the electron

density amplitudes in the these wave fields attain ~1 % and ~10%, respectively, and greater; (8) aperiodic perturbations (for

425   the most part, increases) in the electron density could attain a few tens of per cent.

8 Conclusions

(1) The Harbin Engineering University multifrequency multiple path coherent software defined radio system for probing the ionosphere at oblique incidence have been used to detect the ionospheric effects over the People's Republic of China during the September 29, 2018, to October 6, 2018 super typhoon Kong-Rey event. The movement of the super typhoon was

430   accompanied by significant variations in radio wave characteristics in the 5–10 MHz band.

(2) The ionospheric response to the super typhoon action was clearly observed to occur on October 1–2, 2018 when the typhoon was 2,800–3,300 km away from the propagation path midpoints and the super typhoon Kong-Rey energy gained a maximum value, and on October 5–6, 2018 when the typhoon was 1,000–1,500 km away from the midpoints and its energy decreased by a factor of about 4.

435   (3) The ionospheric effects are more pronounced along the nearest propagation paths, whereas no effect is detected along the propagation path at the farthest distance from the typhoon.

(4) The super typhoon action on the ionosphere was accompanied by the generation or amplification of quasi-sinusoidal variations in the Doppler shift by a factor of 2–3, as well as by noticeable variations in the signal amplitude. The Doppler spectra were observed to broaden in a number of cases.

440   (5) The period of wave perturbations exhibited variability in the ~20 min to ~120 min range. It meant that the perturbations in the ionospheric electron density were caused by atmospheric gravity waves (AGWs) generated by the typhoon: the greater the AGW period, the greater the Doppler shift. As the period increased from 20 min to 120 min, the Doppler shift amplitudes increased from ~0.1 Hz to 0.5–1 Hz.

(6) As the AGW period increases, the amplitude of quasi-sinusoidal variations in the electron density increases from

445   0.4 to 0.6 of per cent.

(7) The Doppler measurements have shown that the dusk terminator and super typhoon acted synergistically to amplify the ionospheric response to these sources of energy.

Code Availability. Software for Passive 14-Channel Doppler radar may be obtained from the website at

450   https://dataverse.harvard.edu/dataset.xhtml?persistentId=doi:10.7910/DVN/MTGAVH (Garmash, 2021).

Data Availability. The data sets discussed in this paper may be obtained from the website at https://dataverse.harvard.edu/dataset.xhtml?persistentId=doi:10.7910/DVN/VHY0L2 (Garmash, 2022).

455

Author Contribution

"**Conceptualization:** Leonid Chernogor; **Data Curation**: Qiang Guo and Kostiantyn Garmash; **Formal Analysis**: All Authors: Yu Zheng, Leonid Chernogor, Kostiantyn Garmash, Qiang Guo, Victor Rozumenko; **Funding Acquisition**: Qiang Guo; **Investigation**: Qiang Guo and Kostiantyn Garmash; **Methodology**: Leonid Chernogor; **Project Administration**: Qiang Guo; **Resources**: Qiang Guo; **Software**: Kostiantyn Garmash; **Supervision:** Leonid Chernogor; **Validation**: All Authors: Leonid Chernogor, Kostiantyn Garmash, Qiang Guo, Victor Rozumenko, Yu Zheng; **Visualization**: Kostiantyn Garmash, Yu Zheng; **Writing – original draft**: All Authors: Leonid Chernogor, Kostiantyn Garmash, Qiang Guo, Victor Rozumenko, Yu Zheng; **Writing review & editing**: All Authors: Leonid Chernogor, Kostiantyn Garmash, Qiang Guo, Victor Rozumenko, Yu Zheng.

Competing Interests. The authors declare that they have no conflict of interests

Acknowledgments

This article makes use of data on typhoon 201825 Kong-Rey recorded by the Japan Meteorological Agency and published at http://agora.ex.nii.ac.jp/digital-typhoon/summary/wnp/s/201825.html.en. The solar wind parameters were retrieved from the Goddard Space Flight Center Space Physics Data Facility https://omniweb.gsfc.nasa.gov/form/dx1.html. This research also draws upon data provided by the WK546 URSI code ionosonde in the city of Wakkanai (45.16° N, 141.75° E), Japan, URL: https://wdc.nict.go.jp/IONO/HP2009/contents/Ionosonde_Map_E.html (ionosonde data are retrieved from http://wdc.nict.go.jp/IONO/HP2009/ISDJ/index-E.html). Work by Qiang Guo and Yu Zheng was supported by the National Key R&D Plan Strategic International Science and Technology Cooperation and Innovation (2018YFE0206500). Work by L. F. Chernogor was supported by the National Research Foundation of Ukraine for financial support (project 2020.02/0015, "Theoretical and experimental studies of global disturbances from natural and technogenic sources in the Earth-atmosphere-ionosphere system"). Work by L. F. Chernogor and V. T. Rozumenko was supported by the Ukraine state research project #0121U109881, and work by K. P. Garmash was supported by the Ukraine state research project #0121U109882.

References

Afraimovich, E. L., Voyeikov, S. V., Ishin, A.B., Perevalova, N. P., and Ruzhin, Yu. Ya.: Variations in the total electron content during the powerful typhoon of August 5–11, 2006, near the southeastern coast of China, Geomag. Aeron., 48, 674–679, https://doi.org/10.1134/S0016793208050113, 2008.

Bortnik, J., Inan, U. S., and Bell, T. F.: Temporal signatures of radiation belt electron precipitation induced by lightning-generated MR whistler waves: 1. Methodology, J. Geophys. Res., 111, A02204, https://doi.org/10.1029/2005JA011182, 2006.

Boška, J. and Šauli, P.: Observations of gravity waves of meteorological origin in the F-region ionosphere, Phys. Chem. Earth. P., C. 26, 425–428, https://doi.org/10.1016/S1464-1917(01)00024-1, 2001.

Chen, J., Zhang, X., Ren, X., Zhang, J., Freeshah, M., and Zhao, Z.: Ionospheric disturbances detected during a typhoon based on GNSS phase observations: a case study for typhoon Mangkhut over Hong Kong, Adv. Space Res., 66, 1743–1753, https://doi.org/10.1016/j.asr.2020.06.006, 2020.

Chernigovskaya, M. A., Shpynev, B. G., and Ratovsky, K. G.: Meteorological effects of ionospheric disturbances from vertical radio sounding data, J. Atmos. Solar-Terr. Phys., 136, 235–243, https://doi.org/10.1016/j.jastp.2015.07.006, 2015.

Chernogor, L. F.: The tropical cyclone as an element of the Earth – atmosphere – ionosphere – magnetosphere system (in Russian), Space Sci. Tech., 12, 16–26, https://doi.org/10.15407/knit2006.02.016, 2006.

Chernogor, L. F.: Advanced Methods of Spectral Analysis of Quasiperiodic Wave-Like Processes in the Ionosphere: Specific Features and Experimental Results, Geomag. Aeron., 48, 652 – 673, https://doi.org/10.1134/S0016793208050101, 2008.

Chernogor, L. F.: Physics and Ecology of Disasters (in Russian), V. N. Karazin Kharkiv National University Publ., Kharkiv, Ukraine, 2012.

Chernogor, L. F., Garmash, K. P., Guo, Q., Luo, Y., Rozumenko, V. T., and Zheng, Y.: Ionospheric storm effects over the People's Republic of China on 14 May 2019: Results from multipath multi-frequency oblique radio sounding, Adv. Space Res., 66, 226 – 242, https://doi.org/10.1016/j.asr.2020.03.037, 2020.

Chernogor L.F., Garmash K.P., Guo Q., Rozumenko V.T., Zheng Y., and Luo Y.: Supertyphoon Hagibis action in the ionosphere on 6–13 October 2019: Results from multi-frequency multiple path sounding at oblique incidence, Adv. Space Res., 67, 2439–2469, https://doi.org/10.1016/j.asr.2021.01.038, 2021.

Chernogor, L. F., Garmash, K. P., Guo, Q., Rozumenko, V. T., Zheng, Y., and Luo, Y.: Disturbances in the ionosphere that accompanied typhoon activity in the vicinity of China in September 2019, Radio Sci., 57. e2022RS007431, https://doi.org/10.1029/2022RS007431, 2022.

Chou, M. Y., Lin, C. C. H., Yue, J., Tsai, H. F., Sun, Y. Y., Liu, J. Y., and Chen, C. H.: Concentric traveling ionosphere disturbances triggered by Super Typhoon Meranti (2016), Geophys. Res. Let., 44, 1219–1226, https://doi.org/10.1002/2016GL072205, 2017.

Chum, J., Liu, J.-Y., Šindelářová, K., and Podolská, T.: Infrasound in the ionosphere from earthquakes and typhoons, J. Atmos. Sol.–Terr. Phys., 171, 72–82, https://doi.org/10.1016/j.jastp.2017.07.022, 2018.

Das, B., Sarkar, S., Haldar, P. K., Midya, S. K., and Pal, S.: D-region ionospheric disturbances associated with the Extremely Severe Cyclone Fani over North Indian Ocean as observed from two tropical VLF stations, Adv. Space Res., 67, 75–86, https://doi.org/10.1016/j.asr.2020.09.018, 2021.

Edemsky, I. K. and Yasyukevich, A. S.: Observing wave packets generated by solar terminator in TEC during typhoons, Solar-Terr. Phys., 4, 33–40, https://doi.org/10.12737/szf-42201806, 2018.

520 Fišer, J., Chum, J., and Liu, J.-Y.: Medium-scale traveling ionospheric disturbances over Taiwan observed with HF Doppler sounding, Earth, Planet. Space., 69, 131, https://doi.org/10.1186/s40623-017-0719-y, 2017.

Freeshah, M., Zhang, X., Şentürk, E., Adil, M. A., Mousa, B. G., Tariq, A., Ren, X., and Refaat, M.: Analysis of Atmospheric and Ionospheric Variations Due to Impacts of Super Typhoon Mangkhut (1822) in the Northwest Pacific Ocean, Remote Sens., 13, 661, https://doi.org/10.3390/rs13040661, 2021.

525 Garmash, K.: Software for Passive 14-Channel Doppler Radar, https://doi.org/10.7910/DVN/MTGAVH, Harvard Dataverse, V1, https://dataverse.harvard.edu/dataset.xhtml?persistentId=doi:10.7910/DVN/MTGAVH, 2021.

Garmash, K.: RAW Data on Parameters of Ionospheric HF Radio Waves Propagated Over China During the September 29 – October 6, 2018 Typhoon Activity in the Vicinity of China, https://doi.org/10.7910/DVN/VHY0L2, Harvard Dataverse, V1 https://dataverse.harvard.edu/dataset.xhtml?persistentId=doi:10.7910/DVN/VHY0L2, 2022.

530 Gavrilov, N. M. and Kshevetskii, S. P.: Dynamical and thermal effects of nonsteady nonlinear acoustic-gravity waves propagating from tropospheric sources to the upper atmosphere, Adv. Space Res. (Includes COSPAR Information Bulletin), 56, 1833–1843, https://doi.org/10.1016/j.asr.2015.01.033, 2015.

Gossard, E. E. and Hooke, W. H.: Waves in the Atmosphere: Atmospheric Infrasound and Gravity Waves, Their Generation and Propagation, Elsevier Scientific Publ. Co., Amsterdam, Netherlands, 1975.

535 Guo, Q., Zheng, Y., Chernogor, L. F., Garmash, K. P., and Rozumenko, V. T.: Ionospheric processes observed with the passive oblique-incidence HF Doppler radar, Visnyk of V.N. Karazin Kharkiv National University, series "Radio Physics and Electronics", 30, 3–15, https://doi.org/10.26565/2311-0872-2019-30-01, 2019a.

Guo, Q., Chernogor, L. F., Garmash, K. P., Rozumenko, V. T., and Zheng, Y.: Dynamical processes in the ionosphere following the moderate earthquake in Japan on 7 July 2018, J. Atmos. Solar-Terr. Phys., 186, 88–103,
540 https://doi.org/10.1016/j.jastp.2019.02.003, 2019b.

Guo, Q., Chernogor, L. F., Garmash, K. P., Rozumenko, V. T., and Zheng, Y.: Radio Monitoring of Dynamic Processes in the Ionosphere Over China During the Partial Solar Eclipse of 11 August 2018, Radio Sci., 55, e2019RS006866, https://doi.org/10.1029/2019RS006866, 2020.

Hickey, M. P., Schubert, G., and Walterscheid, R. L.: Acoustic wave heating of the thermosphere, J. Geophys. Res., 106,
545 21543−21548, https://doi.org/10.1029/2001JA000036, 2001.

Hickey, M. P., Walterscheid, R. L., and Schubert, G.: Gravity wave heating and cooling of the thermosphere: Roles of the sensible heat flux and viscous flux of kinetic energy, J. Geophys. Res., 116, A12326, https://doi.org/10.1029/2011JA016792, 2011.

Hung, R. J. and Kuo, J. P.: Ionospheric observation of gravity-waves associated with Hurricane Eloise, J. Geophys., 45, 67–
550 80, https://journal.geophysicsjournal.com/JofG/article/view/173, 1978.

Inan, U., Piddyachiy, D., Peter, W., Sauvaud, J., and Parrot, M.: DEMETER satellite observations of lightning-induced electron precipitation, Geophys. Res. Lett., 34, L07103, https://doi.org/10.1029/2006GL029238, 2007.

Isaev, N. V., Sorokin, V. M., Chmyrev, V. M., and Serebryakova, O. N.: Ionospheric electric fields related to sea storms and typhoons, Geomag. Aeron., 42, 638–643, 2002.

555 Isaev, N. V., Kostin, V. M., Belyaev, G. G., Ovcharenko, O. Ya., and Trushkina, E. P.: Disturbances of the topside ionosphere caused by typhoons, Geomag. Aeron., 50, 243–255, https://doi.org/10.1134/S001679321002012X, 2010.

Karpov, I. V. and Kshevetskii, S. P.: Numerical study of heating the upper atmosphere by acoustic-gravity waves from local source on the Earth's surface and influence of this heating on the wave propagation conditions, J. Atmos. Solar-Terr. Phys., 164, 89−96, https://doi.org/10.1016/j.jastp.2017.07.019, 2017.

560 Ke, F. Y., Qi, X. M., Wang, Y., and Liu, X. W.: Statistics of ionospheric responses to Southeast Asia's typhoons during 2006-2018 using the rate of change in the TEC index, Adv. Space Res., 66, 1724–1742, https://doi.org/10.1016/j.asr.2020.06.003, 2020.

Kong, J., Yao, Y., Xu, Y., Kuo, C., Zhang, L., Liu, L., and Zhai, C.: A clear link connecting the troposphere and ionosphere: ionospheric reponses to the 2015 Typhoon Dujuan, J. Geod., 91, 1087–1097, https://doi.org/10.1007/s00190-017-1011-4, 565 2017.

Krishnam Raju, D. G., Rao, M. S., Rao, B. M., Jogulu, C., Rao, C. P., and Ramanadham, R.: Infrasonic oscillations in the F2 region associated with severe thunderstorms, J. Geophys. Res., 86, 5873–5880, https://doi.org/10.1029/JA086iA07p05873, 1981.

Kuester, M. A., Alexander, M. J., and Ray, E. A.: A model study of gravity waves over Hurricane Humberto (2001), J. 570 Atmos. Sci., 65, 3231–3246, https://doi.org/10.1175/2008JAS2372.1, 2008.

Li, W., Yue, J., Yang, Y., Li, Z., Guo, J., Pan, Y., and Zhang, K.: Analysis of ionospheric disturbances associated with powerful cyclones in East Asia and North America, J. Atmos. Solar-Terr. Phys., 161, 43−54, https://doi.org/10.1016/j.jastp.2017.06.012, 2017.

Li, W., Yue, J., Wu, S., Yang, Y., Li, Z., Bi, J., and Zhang, K.: Ionospheric responses to typhoons in Australia during 2005– 575 2014 using GNSS and FORMOSAT-3/COSMIC measurements, GPS Solutions, 22, 61, https://doi.org/10.1007/s10291-018-0722-1, 2018.

Luo, Y., Chernogor, L. F., Garmash, K. P., Guo, Q., Rozumenko, V. T., Shulga, S. N., and Zheng, Y.: Ionospheric effects of the Kamchatka meteoroid: Results from multipath oblique sounding, J. Atmos. Solar-Terr. Phys., 207, 105336, https://doi.org/10.1016/j.jastp.2020.105336, 2020.

580 Marple Jr., S. L.: Digital spectral analysis: with applications, Inc, Englewood Cliffs, Prentice-Hall, N. J., XX, 492 p., https://doi.org/10.1121/1.398548, 1987.

Mikhailova, G. A., Mikhailov, Yu. M., and Kapustina, O. V.: ULF-VLF electric fields in the external ionosphere over powerful typhoons in Pacific Ocean, Int. J. Geomag. Aeron., 2, 153–158, http://elpub.wdcb.ru/journals/ijga/v02/gai99321/gai99321.htm, 2000.

585   Mikhailova, G. A., Mikhailov, Yu. M., and Kapustina, O. V.: Variations of ULF-VLF electric fields in the external ionosphere over powerful typhoons in Pacific Ocean, Adv. Space Res., 30, 2613–2618, https://doi.org/10.1016/S0273-1177(02)80358-1, 2002.

Nickolaenko, A. P. and Hayakawa, M.: Heating of the lower ionosphere electrons by electromagnetic radiation of lightning discharges, Geophys. Res. Lett., 22, 3015–3018, https://doi.org/10.1029/95gl01982, 1995.

590   Okuzawa, T., Shibata, T., Ichinose, T., Takagi, K., Nagasawa, C., Nagano, I., Mambo, M., Tsutsui, M., and Ogawa, T.: Short-period disturbances in the ionosphere observed at the time of typhoons in September 1982 by a network of HF Doppler receivers, J. Geomag. Geoelectr., 38, 239–266, https://doi.org/10.5636/jgg.38.239, 1986.

Polyakova, A. S. and Perevalova, N. P.: Investigation into impact of tropical cyclones on the ionosphere using GPS sounding and NCEP/NCAR reanalysis data, Adv. Space Res., 48, 1196–1210. https://doi.org/10.1016/j.asr.2011.06.014, 2011.

595   Polyakova, A. S. and Perevalova, N. P.: Comparative analysis of TEC disturbances over tropical cyclone zones in the north-west Pacific Ocean, Adv. Space Res., 52, 1416−1426, https://doi.org/10.1016/j.asr.2013.07.029, 2013.

Prasad, S. S., Schneck, L. J., and Davies, K.: Ionospheric disturbances by severe tropospheric weather storms, J. Atmos. Terr. Phys., 37, 1357–1363, https://doi.org/10.1016/0021-9169(75)90128-2, 1975.

Pulinets, S. and Davidenko, D.: Ionospheric precursors of earthquakes and global electric circuit, Adv. Space Res., 53, 709–
600   723, https://doi.org/10.1016/j.asr.2013.12.035, 2014.

Šindelářova, T., Burešová, D., Chum, J., and Hruška, F.: Doppler observations of infrasonic waves of meteorological origin at ionospheric heights, Adv. Space Res., 43, 1644–1651, https://doi.org/10.1016/j.asr.2008.08.022, 2009.

Song, Q., Ding, F., Zhang, X., Liu, H., Mao, T., Zhao, X., and Wang, Y.: Medium-scale traveling ionospheric disturbances induced by Typhoon Chan-hom over China, J. Geophys. Res., 124, 2223–2237, https://doi.org/10.1029/2018JA026152, 2019.

605   Sorokin, V. M., Isaev, N. V., Yaschenko, A. K., Chmyrev, V. M., and Hayakawa, M.: Strong DC electric field formation in the low latitude ionosphere over typhoons, J. Atmos. Solar-Terr. Phys., 67, 1269–1279, https://doi.org/10.1016/j.jastp.2005.06.014, 2005.

Suzuki, S., Vadas, S. L., Shiokawa, K., Otsuka, Y., Karwamura, S., and Murayama, Y.: Typoon-induced concentric airglow structures in the mesopause region, Geophys. Res. Lett., 40, 5983–5987,
610   https://doi.org/10.1002/2013GL058087, 2013.

Vanina–Dart, L. B., Pokrovskaya, I. V., and Sharkov, E. A.: Studying the interaction between the lower equatorial ionosphere and tropical cyclones according to data of remote and rocket sounding, Izvestiya, Atmos. Oceanic Phys., 2, 19–27, 2007.

Voss, H. D., Imhof, W. L., Walt, M., Mobilia, J., Gaines, E. E., Reagan, J. B., Inan, U. S., Helliwell, R. A., Carpenter, D. L.,
615   Katsufrakis, J. P., and Chang, H. C.: Lightning-induced electron precipitation, Nature, 312, 740–742, https://doi.org/10.1038/312740a0, 1984.

Voss, H. D., Walt, M., Imhof, W. L., Mobilia, J., and Inan, U. S.: Satellite observations of lightning-induced electron precipitation, J. Geophys. Res., 103, 11,725–11,744, https://doi.org/10.1029/97JA02878, 1998.

Wen, Y. and Jin, S.: Traveling Ionospheric Disturbances Characteristics during the 2018 Typhoon Maria from GPS

620 Observations, Remote Sens., 12, 746, https://doi.org/10.3390/rs12040746, 2020.

Xiao, Z., Xiao, S.-G., Hao, Y.-Q., and Zhang, D.-H.: Morphological features of ionospheric response to typhoon, J. Geophys. Res., 112, A04304, https://doi.org/10.1029/2006JA011671, 2007.

Yiğit, E., Knížová, P. K., Georgieva, K., and Ward, W.: A review of vertical coupling in the Atmosphere–Ionosphere system: Effects of waves, sudden stratospheric warmings, space weather, and of solar activity, J. Atmos. Solar-Terr. Phys., 141, 1−12,

625 https://doi.org/10.1016/j.jastp.2016.02.011, 2016.

Zakharov, V. I. and Kunitsyn, V. E.: Regional features of atmospheric manifestations of tropical cyclones according to ground-based GPS network data, Geomagn. Aeron., 52, 533–545, https://doi.org/10.1134/S0016793212040160, 2012.

Zakharov, V. I., Pilipenko, V. A., Grushin, V. A., and Khamidullin, A. F.: Impact of typhoon Vongfong 2014 on the Ionosphere and Geomagnetic Field According to Swarm Satellite Data: 1. Wave Disturbances of Ionospheric Plasma, Solar-

630 Terr. Physics., 5, 101–108, https://doi.org10.12737/stp-52201914, 2019.

Zakharov, V. I. and Sigachev, P. K.: Ionospheric disturbances from tropical cyclones, Adv. Space Res., 69, 132–141, https://doi.org/10.1016/j.asr.2021.09.025, 2022.

Zhao, Y., Deng, Y., Wang, J.-S., Zhang, S.-R., and Lin, C. Y.: Tropical cyclone-induced gravity wave perturbations in the upper atmosphere: GITM-R simulations, J. Geophys. Res., 125, e2019JA027675,

635 https://doi.org/10.1029/2019JA027675, 2020.

Zhao, Y. X., Mao, T., Wang, J. S., and Chen, Z.: The 2D features of tropical cyclone Usagi's effects on the ionospheric total electron content, Adv. Space Res., 62, 760–764, https://doi.org/10.1016/j.asr.2018.05.022, 2018.